
# Local and global effects on the diurnal variation of the atmospheric electric field in South America by comparison with the Carnegie curve

J. Tacza, J.-P. Raulin, E. Macotela, A. Marun, G. Fernandez, F.C.P. Bertoni, L.M. Lima, J. Samanes, Y. Buleje, E. Correia, G. Alves, K. Makita

PII: S0169-8095(19)31323-7

DOI: https://doi.org/10.1016/j.atmosres.2020.104938

Reference: ATMOS 104938

To appear in: *Atmospheric Research*

Received date: 13 October 2019

Revised date: 2 February 2020

Accepted date: 1 March 2020

Please cite this article as: J. Tacza, J.-P. Raulin, E. Macotela, et al., Local and global effects on the diurnal variation of the atmospheric electric field in South America by comparison with the Carnegie curve, *Atmospheric Research*(2019), https://doi.org/10.1016/j.atmosres.2020.104938

# Local and global effects on the diurnal variation of the atmospheric electric field in South America by comparison with the Carnegie curve

J. Tacza[1*], J.-P. Raulin[1], E. Macotela[2], A. Marun[3], G. Fernandez[4], F. C. P. Bertoni[5], L. M. Lima[5], J. Samanes[6], Y. Buleje[7], E. Correia[1,8], G. Alves[9,10], K. Makita[11]

1. Center of Radio Astronomy and Astrophysics, Engineering School, Mackenzie Presbyterian University, São Paulo, Brazil.

2. Sodankyla Geophysical Observatory, University of Oulu, Sodankyla, Finland.

3. Instituto de Ciencias Astronómicas de la Tierra y el Espacio, San Juan, Argentina.

4. Complejo Astronómico El Leoncito, CASLEO, San Juan, Argentina.

5. Departamento de Física, Universidade Estadual da Paraíba, Campina Grande, Brazil.

6. Dirección de Astrofísica, Comisión Nacional de Investigación y Desarrollo Aeroespacial, Lima, Peru.

7. Universidad Nacional San Luis Gonzaga de Ica, Ica, Peru.

8.Instituto Nacional de Pesquisas Espaciais, Ministério de Ciência e Tecnología, São José dos Campos, Brazil.

9. Universidade Federal de Roraima, Boa Vista, Brazil.

10. Instituto Federal de Roraima, Campus Amajari, Brazil.

11. Takushoku University, Tokyo, Japan.

* Corresponding author:

E-mail address: josect1986@gmail.com

Full postal address: Center of Radio Astronomy and Astrophysics, Engineering School, Mackenzie Presbyterian University, São Paulo, SP, Brazil

**Author Statement**

**José Tacza:** Conceptualization, Methodology, Investigation, Formal Analysis, Writing - Original draft. **Jean-Pierre Raulin:** Supervision, Resources, Writing - Review & Editing, Funding Acquisition. **Edith Macotela:** Software, Investigation, Data Curation, Writing - Review & Editing. **Adolfo Marun, Germán Fernandez, Fernando Bertoni, Lourivaldo Lima, Jorge Samanes, Yovanny Buleje, Emilia Correia, Gilmar Alves, Kazuo Makita:** Data Curation, Investigation, Writing - Review & Editing

**Abstract:** The study of the global atmospheric electric circuit is important to understand the climate system and this can be done by monitoring the atmospheric electric field worldwide. In this way, continuous measurements of atmospheric electric field are being recorded by the Atmospheric electric FIeld Network in South America (AFINSA). The main objective of this network is to obtain the daily curve of atmospheric electric field variations under fair weather conditions for each station, through monthly, seasonal and annual averages. These curves are called 'standard curves'. In this paper, we compare and analyze the monthly, seasonal and annual standard curves for each sensor location. The results indicate significant similarities and differences between the annual standard curve and the Carnegie curve. The similarities, with correlation $r \geq 0.9$ for most stations, are associated with a global representation of the global electrical circuit and the differences due to local effects, such as 'Austausch' effect and pollution.

## 1. Introduction

The Atmospheric Electric Field (AEF) persists in regions of fair weather and shows a typical daily variation. In the beginning, 'fair weather' was known as 'serene weather' (Bennett and Harrison, 2007). It was initially classified based on the AEF records: '0' type, no negative AEF recorded, '1' type, one or more hours with negative AEF values for less than three hours, and '2' type, negative AEF measurements with more than three hours of duration (Whipple, 1937; Harrison and Nicoll, 2018). Since 1964 the United Kingdom Meteorological Office defined 'fair weather' conditions as those without hydrometeors, with no low stratus cloud, less than three-eighths cumuliform cloud and a mean hourly wind speed of less than 8 m/s (Harrison, 2013). Recently, Harrison and Nicoll (2018) proposed these requirements as follows: the absence of hydrometeors, aerosol and haze, negligible cumuliform cloud present and no extensive stratus cloud with its cloud base below 1.5 km and surface wind speed between 1 m/s and 8 m/s.

In the early twentieth century, hourly averaged measurements of AEF over the world's ocean were performed by the Carnegie Institution of Washington (Torreson et al., 1946), especially those made by the cruise VII between 1928-1929, showed a typical daily variation in fair weather conditions, which was independent of the ship's position in Universal Time. This daily variation is known as the Carnegie curve and it is used to be considered as the 'universal' curve in fair weather conditions (Harrison, 2013). Questions arose about the origin and how the AEF is maintained.

Wilson (1903, 1921) proposed that the AEF in fair weather conditions is originated and maintained by thunderstorms and electric shower clouds activity occurring in remote regions. The relationship between these parameters form part of the concept of the Global Atmospheric Electric Circuit (GAEC). The circuit is formed between the Earth's surface and the lower atmosphere (Haldoupis et al., 2017) and it relates separation of charges in disturbed weather with a current flowing in fair weather regions (Wilson, 1921). In the GAEC model, there are ascending vertical currents above thunderstorms and electrical shower clouds (disturbed weather regions), which flow from the cloud's top to the atmosphere. This current flows freely through the highly conductive ionosphere and flows down from the atmosphere to the ground in fair weather regions. Finally, the GAEC is closed by currents that flow from fair weather to disturbed weather regions through the rocks and the oceans of the Earth's surface (Rycroft et al., 2000; Rycroft et al., 2008). The GAEC model is supported by the comparison between the Carnegie curve and the electrical activity, i.e. thunderstorms and electrical shower clouds (Whippel, 1929; Liu et al., 2010; Mach et al., 2011; Peterson et al., 2017).

The importance of studying the global electric circuit is summarized in the reviews done by Williams (2009) and Williams and Mareev (2014). These topics include the contribution of mesoscale convective system to the GAEC, global effects of nuclear weapon tests, response to the climate change, the role of lightning in the GAEC, among other phenomena. Furthermore, the GAEC may act as the link between the space weather and the lower atmosphere (Rycroft et al., 2012; Nicoll and Harrison, 2014; Tacza et al., 2018). Thus, the continuous monitoring of the GAEC is important and this can be done indirectly by monitoring the atmospheric electric field on the ground in fair weather conditions.

As mentioned before, the Carnegie curve is closely related to the GAEC. Then, it is usually used as the reference curve of the AEF, in fair weather conditions, when looking for global effects. The Carnegie curve shows a minimum at 3 UT and a maximum at 19 UT. It has a mean value of ~130 V/m and an amplitude variation of ~35%. This curve was obtained averaging the measurement taken during several days in different years and over the oceans (Harrison, 2013). Nonetheless, mean daily variation of the AEF performed in polar regions have shown great similarity with the Carnegie curve (Kasemir, 1972; Reddell et al., 2004; Burns et al., 2005; Burns et al., 2012; Jeeva et al., 2016; Kubicki et al., 2016; Burns et al., 2017). For instance, Burns et al. (2012) found almost a perfect correlation in shape and amplitude between the AEF mean curve obtained at Vostok (Antarctica) and the Carnegie curve. Similar results were found at Concordia, 560 km away of Vostok (Burns et al., 2017). At Henryk Arctowsky Antarctica station, Kubicki et al. (2016) found a correlation coefficient of 0.75 between the AEF mean curve and the Carnegie curve, with a maximum at 19-20 UT, which usually corresponds with the maximum thunderstorm activity in the American sector. At the South Pole station, Reddell et al. (2004) found a maximum at 1830 UT and a minimum at 3 UT. Jeeva et al. (2016) found three types of curves in fair weather conditions at Maitri station. Type 1 was very close to the Carnegie curve while the other types showed clearly differences associated to katabatic winds. Similarly, at Greenland, in the Arctic pole, Kasemir (1972) found a close AEF mean curve when compared with the Carnegie curve.

Measurements of AEF were also performed over the oceans after the Carnegie cruises. Takagi and Kanada (1972) performed measurements of AEF in the middle and south Pacific Ocean. The authors found a close relationship with the Carnegie curve. Similar results were found by Morita (1971). However, Manohar et al. (1990) found departures in their mean curves performed at the Arabian Sea, Indian Ocean and Bay of Bengal regions. The authors

associated these differences to the presence of aerosols near to the coast. AEF measurements around cities, also present departures, in shape and amplitude, when compared with the Carnegie curve. They are believed to be due to local factors as the 'Austausch effect', meteorological variables, pollution, etc. (Israël, 1959; Anderson and Trent, 1969; Israël, 1970; Bhartendu, 1971; Tuomi, 1989; Kamra et al., 1994; Harrison and Aplin, 2002; Harrison, 2006; De et al., 2013; Xu et al., 2013; Silva et al., 2014; Yaniv et al., 2016; Lucas et al., 2017; Gurmani et al., 2018). In order to minimize local effects, measurements of AEF have been performed at remote regions from cities as mountains (Tacza et al., 2014; Kamogawa et al., 2016; Yaniv et al., 2017) and islands (Cobb, 1968; Lopes et al., 2017).

In the search for global effects on the AEF variability it is important to monitor AEF in different places around the world. With this objective in mind, several regional networks to measure the AEF are being developed in North America (Lucas et al., 2017), Pakistan (Gurmani et al., 2018), Israel (Yaniv et al., 2016; Yaniv et al., 2017), Antarctica (Jeeva et al., 2016; Burns et al., 2017) and South America (Tacza et al., 2014). Some of these sensor's locations, and new ones worldwide, are grouped to form part of the GLOCAEM (Global Coordination of Atmospheric Electricity Measurements) network, which is an international collaborative effort towards an effective global network for atmospheric electricity monitoring (Nicoll et al., 2019).

In this paper, we present AEF mean curves from a network of electric field mill sensors installed in South America, which is called Atmospheric electric FIeld Network in South America (AFINSA). Details of the AFINSA network are presented in section 2. The data analysis is explained in section 3. Results and discussions about the similarities and

differences between the AEF mean curve for AFINSA network and the 'universal' Carnegie curve are presented in section 4. The final section summarizes the main remarks of this paper.

## 2. The AFINSA Network

Continuous measurements of the atmospheric electric field are being recorded by several Electric Field Mill (EFM) sensors installed at different stations in South America. These sensors form part of the Atmospheric electric FIeld Network in South America (AFINSA, https://theafinsa.wordpress.com). The network was created with the purpose of measuring AEF daily variation in fair weather conditions in order to analyze the impacts of different geophysical and solar phenomena (Tacza et al., 2014). The following is a brief explanation of the EFM sensors and their location.

### 2.1 EFM Sensors

Each sensor consists of a Boltek EFM-100. The principle of operation is very simple: when a conducting plate is exposed to an electric field, a charge is induced proportional to the electric field and area of the plate (Imyanitov, 1957; Secker, 1975; MacGorman and Rust, 1998). The dynamic range of the EFM is ±20 kV/m. Electric field measurements are recorded with a time resolution of 0.05 s. These EFM sensors measure the potential gradient (PG=$-E_z$, where $E_z$ is the vertical AEF). Throughout the paper, PG measurements will be described as AEF measurements.

### 2.2 The Network

The AFINSA network consist of 9 EFM sensors installed at different places over South America: CAS (El Leoncito, San Juan, Argentina, two sensors separated by ~400 meters), ICA (Ica, Peru), PLO (Lima, Peru), HYO (Huancayo, Peru), ROR (Boa Vista, Brazil), CGR and LSA (Paraíba, Brazil, both sensors ~12.5 km apart) and SPA (São Paulo, Brazil). Table 1 shows the ID name, geographical coordinates, altitude and a brief description of the stations. Figure 1 shows a map with the position of the sensors already installed (triangles) and the new station to be installed in Moquegua city (Peru) by 2020 (star).

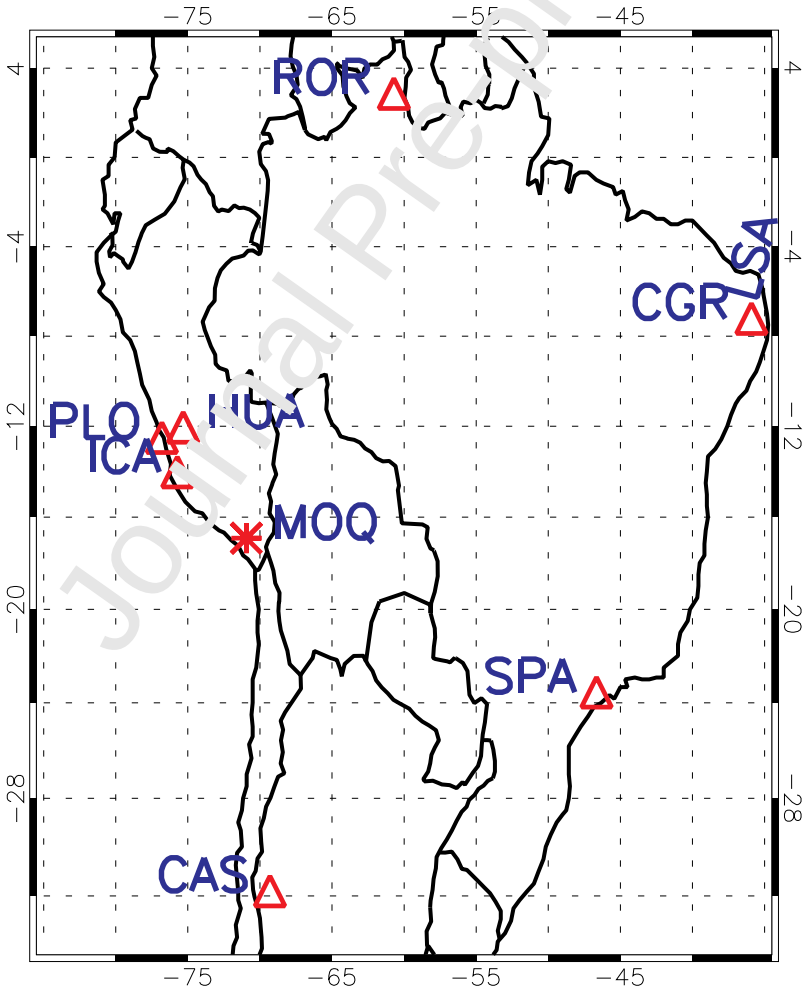


Figure 1. The AFINSA network. Triangles indicate sensors already installed and star future location for a new sensor.

## 3. Data analyses

The EFM sensors needs to be positioned at ground level to avoid overestimating of the AEF values due to the peak effect (Chubb, 2014). However, this is impractical because the sensor can be damaged by animals, dirt, water, etc. Thus, usually at many locations the EFM sensor is placed at a certain height above the ground surface resulting in overestimated readings. To fix that, simultaneous recording was performed using a second EFM sensor collocated at the ground level. The linear regression between both sensors outputs was calculated and used to correct AEF values. This process is shown for CAS station in Tacza et al. (2014). This methodology was performed for stations: CAS, ICA, PLO and HYO. For ROR, CGR, LSA and SPA stations, it was not possible to perform simultaneous measurements, and therefore, AEF intensities were not corrected yet. However, this does not exclude its analysis for the purpose of this paper.

After correcting the AEF values, the first step consists in choosing the AEF daily curve in fair weather conditions. We adopt a criterion that does not consider meteorological conditions because for most of the AEINSA sensors there is not a meteorological station nearby. Thus, a simple criterion was adopted by choosing a range of AEF positive values based on the histograms performed for each station and shown in Figure 2. In accordance with Figure 2, the range of amplitude (in V/m) are: CAS (0-200), ICA (0-200), PLO (0-250), HYO (0-200), CGR (0-500), LSA (0-1000), ROR (0-1000) and SPA (0-3000). The higher values for CGR, LSA, ROR and SPA stations are due to the fact that data were not corrected for the positon of the sensor, therefore producing an overestimated value, as mentioned above. In addition, SPA station has very high AEF values, possibly due to the presence of pollution, owing that the EFM sensor is located at the center of the São Paulo city and is more sensitive to vehicular

traffic. CGR and LSA stations present negative values, mainly observed between October and March, every year, possibly associated to the rainy season in North East of Brazil. Then, this period of time will not be considered in our analysis. On the other side, note that the mean value for the stations where the AEF values were corrected is ~100 V/m which is consistent with values reported on the ground level in fair weather conditions (Israël, 1970; Nicoll et al., 2019 and references therein).

To validate this simple observational criterion, annual averages of AEF daily curve were obtained and compared with annual averages obtained using a meteorological criterion, which was to choose days with wind speed < 8 m/s and no rain. The comparison was performed for 2016 AEF data recorded at HYO station. We used data from a meteorological station located ~ 200 meters away from the HYO EFM sensor. Figure 3 compares the mean annual AEF daily curve using our criterion (red line) and that obtained using the meteorological criterion (black line). The error bars represent one standard deviation (1σ) of the mean. A high similarity between both curves is found. The linear correlation coefficient is $r = 0.99$. This comparison validates our criterion, which is a good representation of 'fair weather' conditions and the same will be used in places where meteorological stations are not available. Furthermore, Figure 3 also shown in blue curve the AEF historical data recorded at HYO station[1] during 6 days in October 1929 (Torreson and Wait, 1948). It is observed the great similarity between historical and current measurements of AEF, $r = 0.96$ compared with the observational curve and $r = 0.95$ with the meteorological curve.

Figure 4 shows typical AEF daily curves for all stations of the AFINSA network, with 1 minute averaged, obtained using our criterion to define 'fair weather' days. These curves

[1] The HYO station is located at Huancayo Observatory (Lat. -12.04°, Long. -75.32°) that belongs to Geophysical Institute of Peru (IGP). Electrical measurements were performed by the Carnegie Institution of Washington in this observatory during 1924-1934 (Torreson and Wait, 1948)

considered as the typical 'fair weather' curves, will be used to produce monthly, seasonal and annual averages. These averaged curves are called 'standard curves'. The total number of 'fair weather' days for each station is indicated in Table 2. As explained before, CGR and LSA stations record a large quantity of AEF negative values during October to March, so, for this period there are zero fair weather days. Similarly, at HYO station there are high occurrence of rainy and cloudy events between October and April (Saavedra and Takahashi, 2017; Saavedra et al., 2020) and this is the reason of the few 'fair weather' days. For HYO station, the '-' symbol means that for these months there was no AEF data.

From Figure 4, it is observed the differences between the AEF values for all stations due to AEF measurements have not been corrected for site distortion factors in each station. In order to compare our curves, throughout the paper we used the AEF values with respect to the mean value at each station (AEF as percentage of the mean).

## 4. Results and discussions

### 4.1 Comparing "standard curves" for the stations of AFINSA network

The first purpose of this paper is to compare the standard curves of the AFINSA network in order to analyze local and global effects. Figures 5, 6 and 7 show the monthly, seasonal and annual standard curves, respectively, for all stations, in percentage of the mean using 1-hour average data. For Figure 5, it is shown a similarity between the monthly standard curves for all AFINSA stations. Particularly for the months of May, June, July and August (winter season in the South Hemisphere) the agreement between the shape and amplitude variation of the curves are evident. On the other hand, for months of December, January and February

(summer season in the South Hemisphere) there are differences in shape and amplitude. These features are more evident in the seasonal standard curves (Figure 6).

Tables 3, 4 and 5 show the linear correlation coefficient 'r' between standard curves for all stations of AFINSA network obtained by month, season and year, respectively. In addition, Table 5 shows the linear correlation coefficient between the annual standard curves for AFINSA stations with the Carnegie curve. While a high correlation coefficient suggests that global effects are dominant, a weaker coefficient indicates that the standard AEF curves are affected by local effects.

The similarities between the standard curves will be discussed further in the next section. Following we discuss the differences between the monthly, seasonal and annual standard curves of the AFINSA stations due to local effects. Emphasis is given to Figure 5 and Table 3 since the same comments are valid for Figure 6 and Table 4, and for Figure 7 and Table 5.

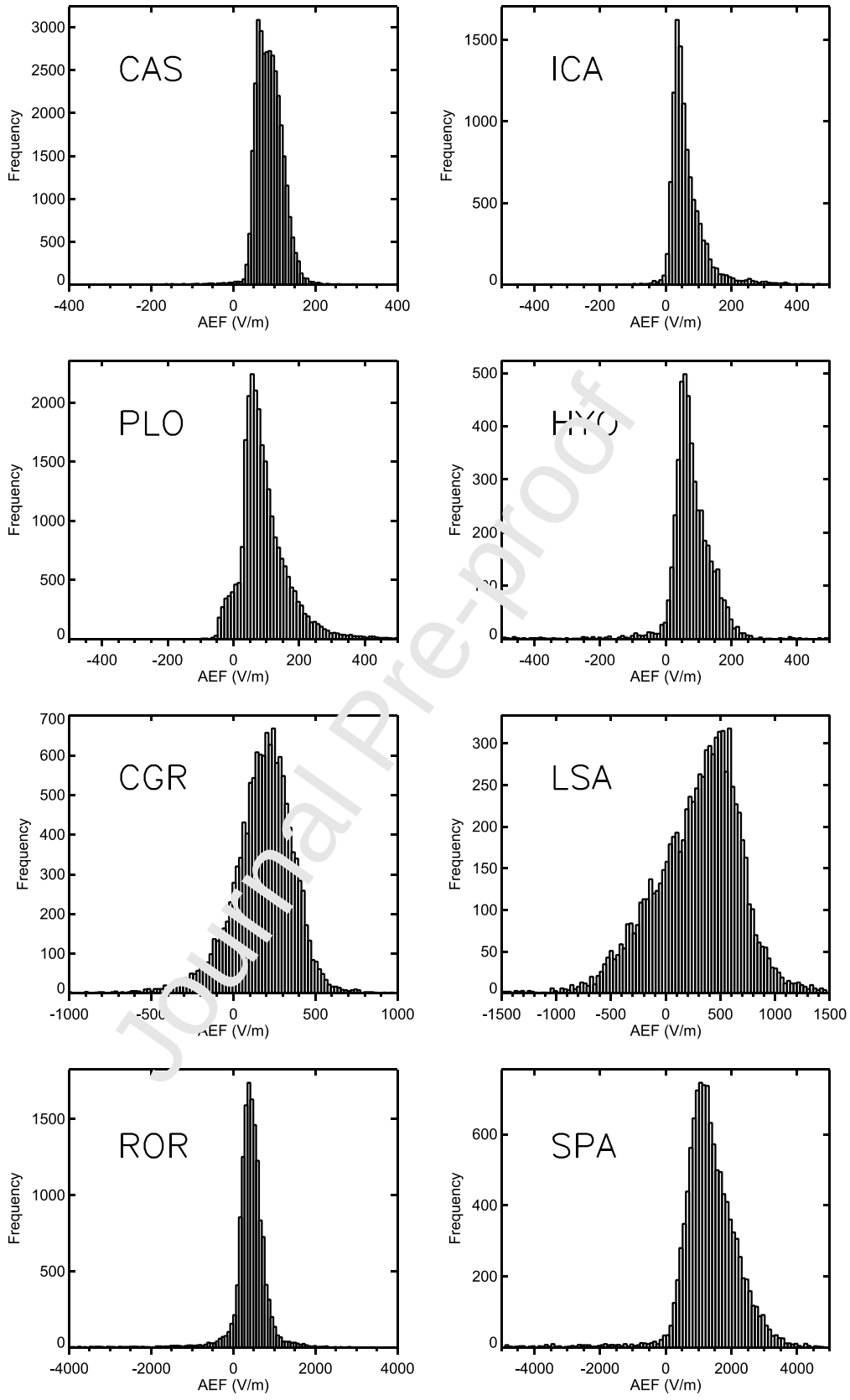


Figure 2. Atmospheric electric field histograms for all stations of AFINSA network.

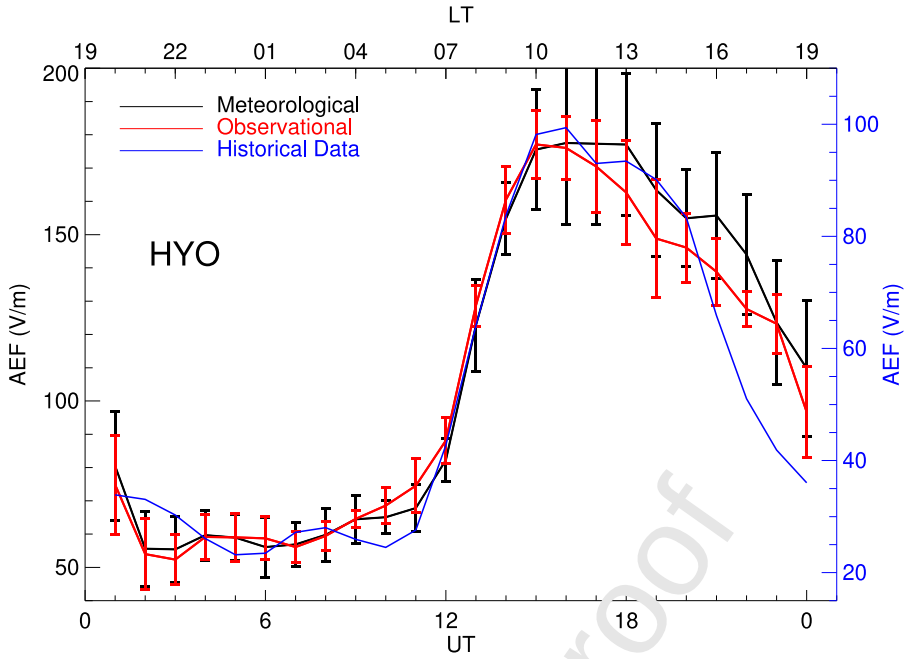


Figure 3. Comparison between the annual averages of the atmospheric electric field daily curve for the observational (red curve) and meteorological (black curve) criteria. The error bars are one standard deviation of the mean, 1σ. The blue curve is the historical data recorded during 6 days in October 1929 (Torreson and Wait, 1948).

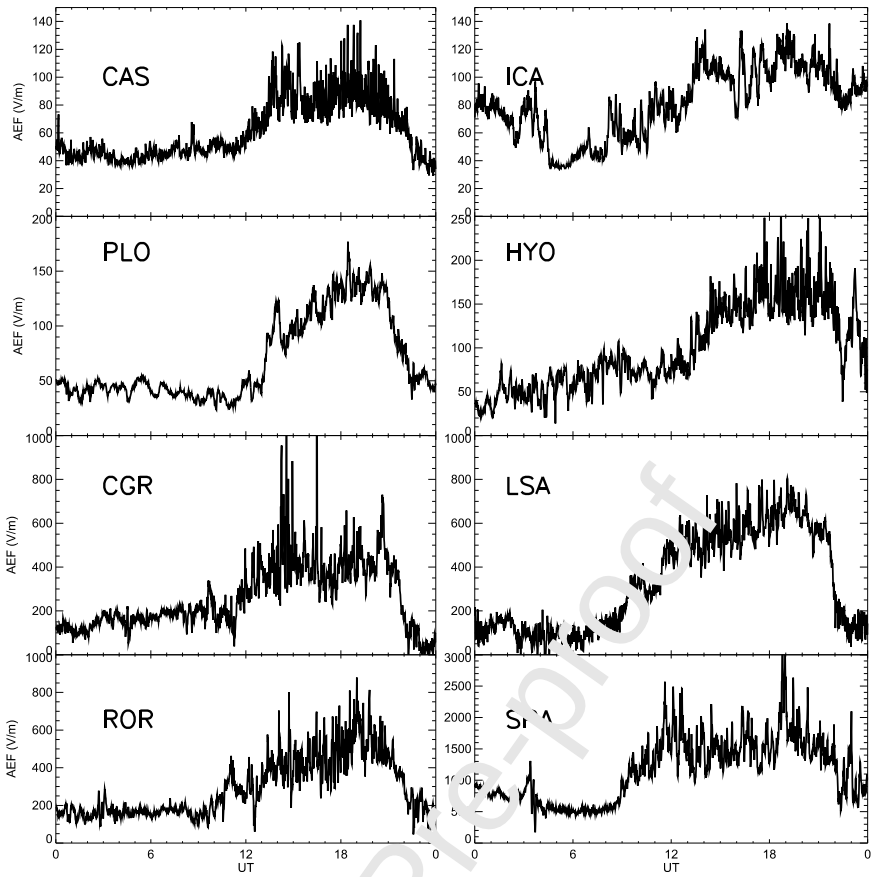


Figure 4. Typical atmospheric electric field daily variation in 'fair weather' days for all stations with 1 minute averaged.

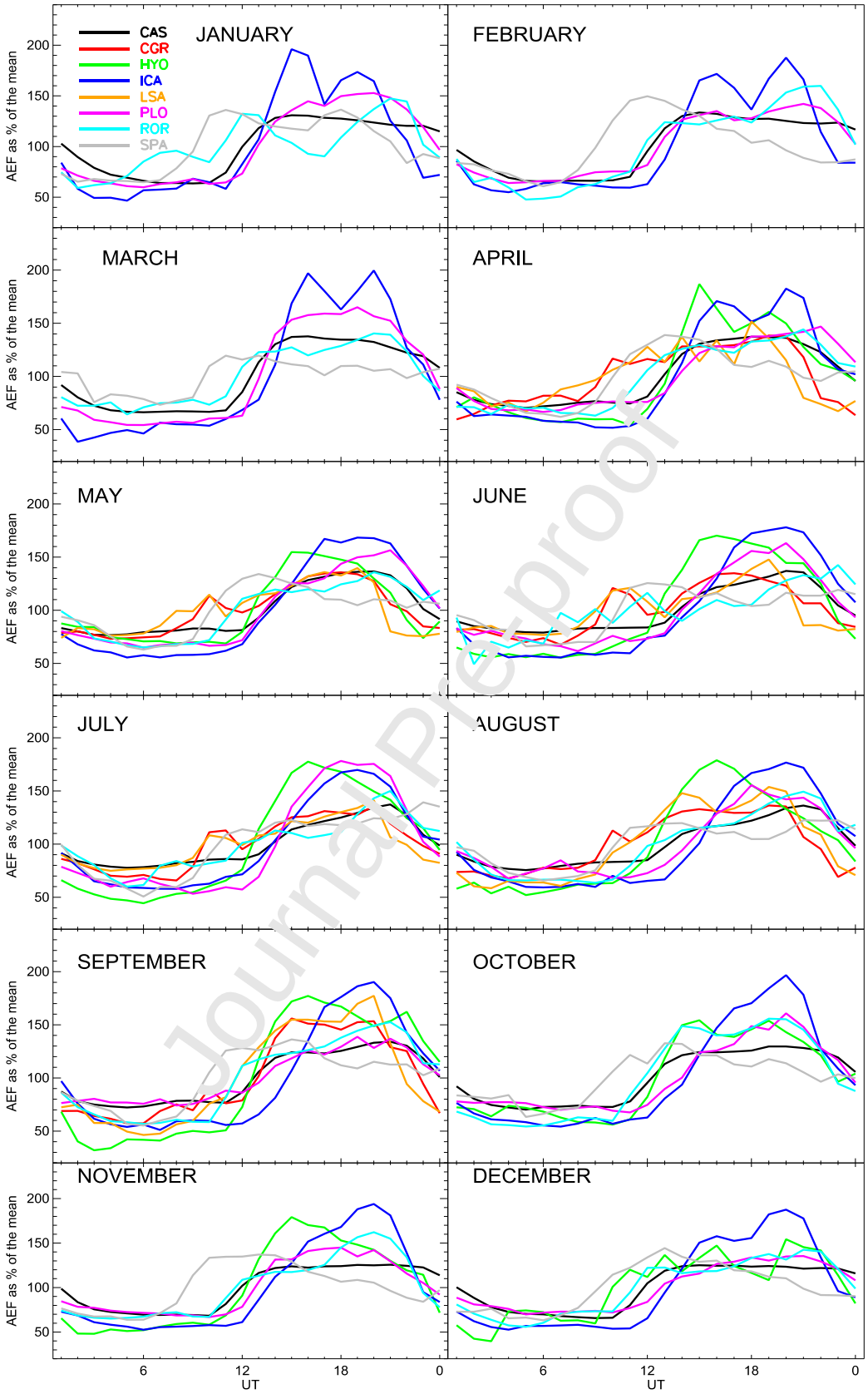


Figure 5. Monthly standard curve, plotted as a percent of the mean, for all stations of AFINSA network.

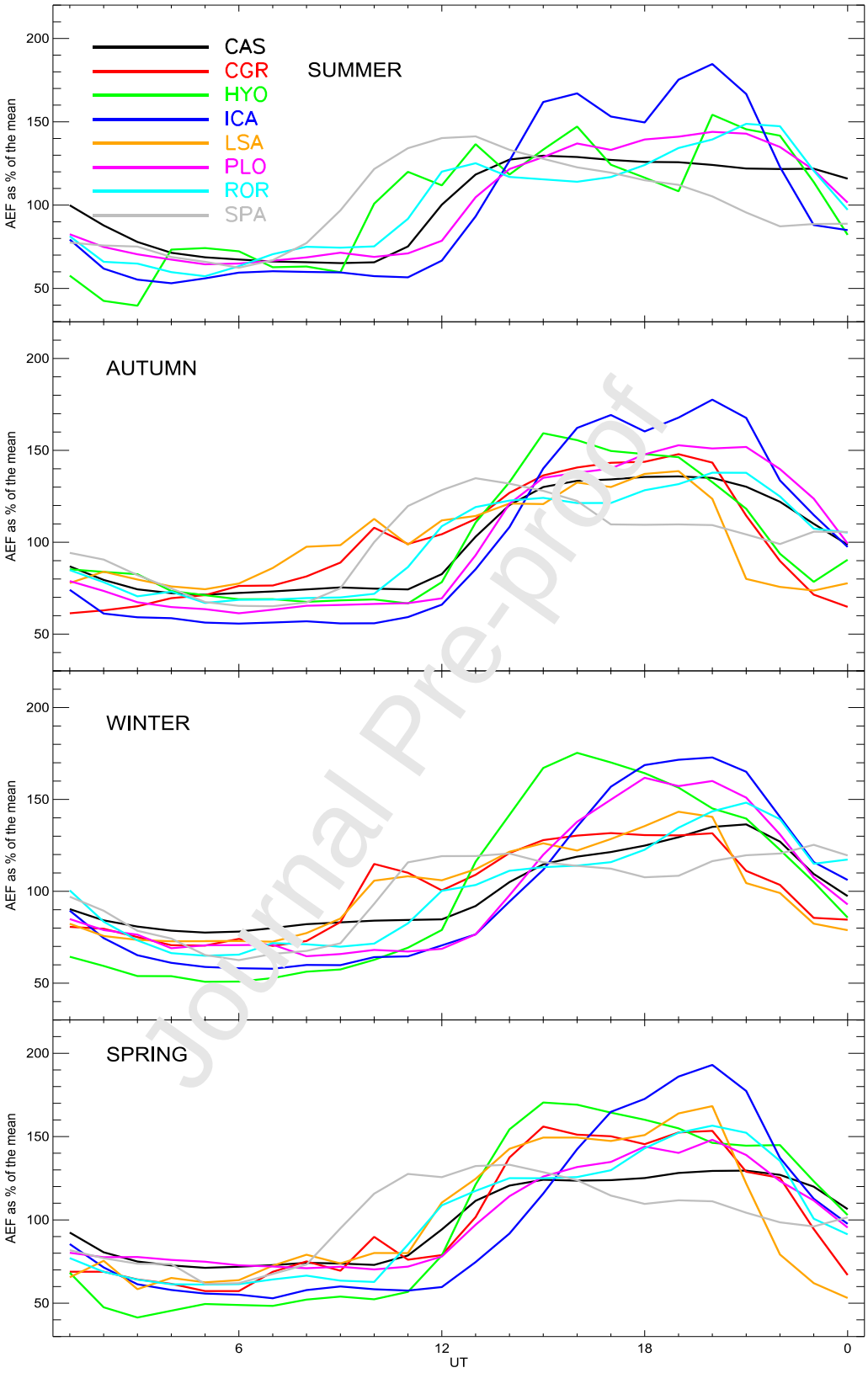


Figure 6. Seasonal standard curve, plotted as a percent of the mean, for all stations of AFINSA network.

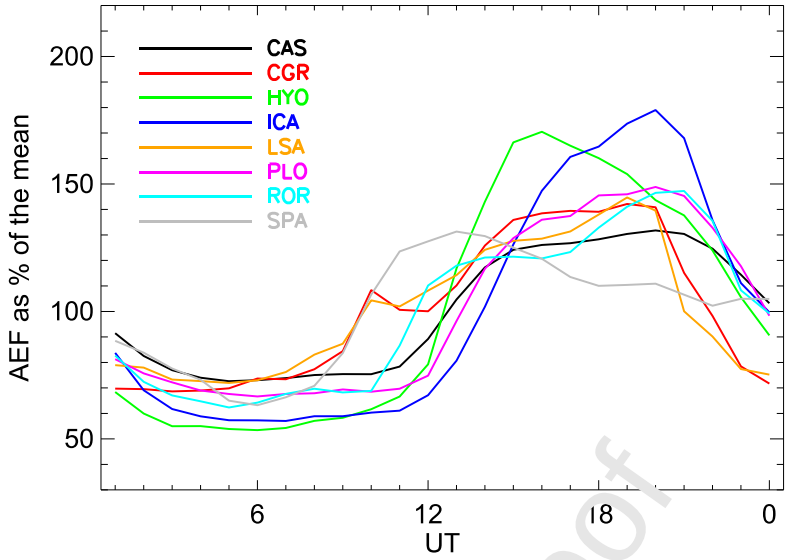


Figure 7. Annual standard curve, plotted as percent of the mean, for all stations of AFINSA network.

**Meteorological variables.** Local effects due to meteorological phenomena is one of the main factors influencing the atmospheric electric field (Bennett and Harrison, 2007). Unfortunately, for most of the AFINSA network stations, a meteorological station is not available yet, but as explained before, the observational criterion to choose 'fair-weather' days should discard 'disturbed' days affected mainly by thunderstorms, strong charge clouds and rain. For example, for CGR and LSA stations, it is reported negative AEF values between October and March. Therefore, for these months there are zero fair weather days (Table 2). Furthermore, the hourly average and the average of several days should remove local meteorological transient effects. It is supported, for example, by the correlation between the standard curves for CAS, ICA and PLO where it is found $r \geq 0.83$ for all months. Monthly standard curve for HYO station also has $r \geq 0.72$ when compared with the standard curves for CAS, ICA and PLO station for all months. CGR and LSA station has $r \geq 0.83$ between their monthly standard curves for all months. Monthly standard curve for ROR station shows $r \geq 0.8$

for September and weak correlation for January when compared with the other stations. It is worth to note that r increases for seasonal and annual standard curve between all stations of the AFINSA network (Table 4 and 5). Still, annual standard curve for SPA station remains between $0.5 \leq r \leq 0.75$ when compared with the other stations. This can be due to an effect of anthropogenic pollution.

**Effect of pollution.** Another main local factor influencing the AEF is the anthropogenic pollution, such as vehicular traffic. Aerosol particles of pollution attach to ions in the atmosphere decreasing the electrical conductivity and by Ohm's law producing AEF increases. This effect has been evidenced in several works (Anderson and Trent, 1969; Israël 1970; Harrison and Aplin, 2002; Harrison, 2006; Silva et al., 2014; Gurmani et al., 2018). Of course, the larger the city, the larger the effect. As mentioned before, Table 3 indicates that the monthly standard curve of SPA station has a weak correlation with the other monthly standard curves of AFINSA network for some months, being February and November the weaker correlations. This because SPA station is located at the center of São Paulo city and it is influenced by pollution (vehicular traffic). This is evidenced in Figure 5 where the peak of the AEF values at 10-12 UT (07-09 LT) corresponds to the rush hour. The same explanation can be valid for HYO station, which shows a peak at 15-16 UT (10-11 LT). It is interesting to note that historical data performed ~90 years ago also shows a similar peak (Figure 3). Further comparison between AEF historic and current measurements, at HYO station, can be useful as proxy of air pollution measurements (Harrison, 2006; Aplin, 2012). Thus, we plan to perform such research as a follow up. Unlike to SPA station, the monthly standard curve of HYO station has a good correlation with the other stations of AFINSA network. This difference with SPA station can be due to HYO station is located at 15 km of Huancayo city while SPA station is located at the center of São Paulo city. Therefore, it is expected more

influence of pollution at SPA station. In addition, this effect also seems to be observed in ICA station, which is located at Ica city. The monthly standard curve for ICA station seems to be perturbed by pollution at 15-16 UT (LT-5) which is intensified during the months of January until April and with less intensity in December. Despite of this, ICA also shows a good correlation with the other stations. For the other stations of the AFINSA network it seems that an effect of anthropogenic pollution is less significant. It is worth no note that Sao Paulo is a big city in comparison with the other localities. Furthermore, it is assumed that the hourly average and the average of several days should remove transient local effects, which was supported by the high correlation coefficient between some of the station of AFINSA network, e.g., r≥0.9, for CAS, ICA and PLO stations.

**'Austausch' Process and Sunrise effect.** The 'Austausch' process is the transport of electric charges in the lower layer of the atmosphere due to an increase of turbulence (Kasemir, 1972; Yaniv et al., 2017). Israël (1959) defined this process as 'electric agitation', which is a strong 'agitation' overlapping the global diurnal variation, which increases with sunrise, reaching a maximum about midday, and falling towards the evening. At nighttime, under low wind speed conditions and low turbulence, electrical charges may accumulate in the first few meters of the earth's surface due to the electrode effect. At sunrise, the soil surface begins to heat up producing convection and turbulence, which produces an increase in the AEF. This can be understood as follows: at sunrise, temperature increases generating convection and turbulence on the earth's surface, thus producing an increase in the aerosol concentration. This increase can result from two processes: bonding between the ultrafine aerosol particles growing in size and/or attachment of small atmospheric ions with aerosol particles, decreasing their concentration (Yaniv et al., 2016; Yaniv et al., 2017). The decrease in the percentage of ions can be approximately 33%, depending mainly on soil type (Kamsali et al.,

2011). The decrease in ion concentration produces a decrease in electrical conductivity and increases the atmospheric electric field (by Ohm's law). Additionally, there can be an increase in the space charge, which is accumulating at the top of the planetary boundary layer (Nicoll et al., 2018). The mentioned processes can result in an increase of the atmospheric electric field of approximately 10-100 V/m (Anisimov et al., 2018). Furthermore, some authors reported a sharp increase of the AEF beginning shortly after the sunrise, which is known as the 'sunrise effect'. These unusual events tend to occur when the wind is calm, the relative humidity is high and the ground is moist. Its duration is about 1h and reach AEF values between 2-4 times the normal fair weather values (Marshall et al., 1999; Smirnov et al., 2012). Figure 8 shows the standard annual curves for all stations of AFINSA network in local time. It is clear to note that the AEF increases in the range 6-8 LT for all stations, that is at local sunrise. The AEF reaches a maximum at different times for the different stations and decreases at night time. As Israël (1959) pointed out the 'Austausch' process is superimposed to the global diurnal variation. Thus, we can assume that the atmospheric electric field recorded at any place includes the contributions of local and global effects, and thus can be represented as $E_T = E_G + E_L$, where $E_T$ is the total atmospheric electric field, $E_G$ is the global component of the AEF and $E_L$ is the local component of the AEF. The contribution of the local component will depend on several factors, such as meteorological conditions, the ionization rate produced by the earth's surface, aerosol concentration and local pollution. In the next section, it will be discussed more about the global component of the AEF in our measurements.

Finally, we believe important to remember that the standard curves will be useful to identify and quantify deviations due to different geophysical and solar phenomena (Tacza et al., 2014; Tacza et al., 2016; Tacza et al., 2018; Nicoll et al., 2019).

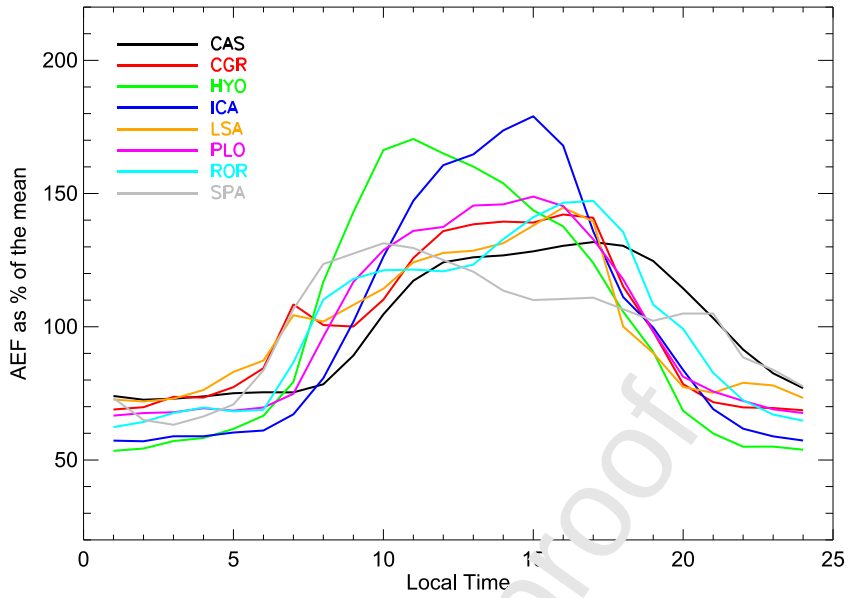


Figure 8. Same as Figure 7 but in Local Time for each station of AFINSA network.

### 4.2 Comparison with the "universal" Carnegie curve

The second purpose of this paper is the comparison between the annual standard curves for all stations of AFINSA network with the 'universal' Carnegie curve. This is shown in Figure 9, where the annual standard curves (black curve) for all stations and the Carnegie curve (red curve) are shown in percent of the mean. The low and top axes represent Universal and Local Time, respectively. Vertical lines indicate the sunrise and sunset time, respectively, for each measurement site.

In Figure 9, we do observe a great similarity in shape between the annual standard curves and the Carnegie curve for all stations, supported by the high correlation coefficient ($r \geq 0.86$) between them (see Table 5) except for SPA station ($r=0.66$). Figure 9 also reveals that the AEF peak maximum occurs at the same time as the maximum of the Carnegie curve, for all

stations (except SPA and HYO station). This peak is at ~20UT and represents the peak of thunderstorm variation in South America. Furthermore, a great similarity between the curves is found between 12-24 UT, which suggests a global effect during this period. However, SPA and HYO stations have some significant differences at the same time. As mentioned in the previous subsection, SPA and HYO station are influenced by anthropogenic pollution (vehicular transit) and this is the reason why the peak maxima of the AEF are different. On the other hand, during the period 00 - 11 UT the majority of the AFINSA's sensors do not measure the characteristic peak of thunderstorm variation in Asia. This could be because the long distance between the Asian generator system and the AFINSA sensors. In fact, AEF measurements on the Indian Ocean shows a trend towards greater effects in the AEF due to storm activity on Asia-Australia and Africa-Europe and weak effects for distant storms occurring in the Americas (Kamra et al., 1994).

On the other hand, from Figure 9 it is evident a clear difference of the amplitude variation of both the standard and the Carnegie curves. At this point, it is important to have in mind that the amplitude variation of the Carnegie curve is ~35%, which is almost the same as the thunderstorm and electric shower clouds (Peterson et al., 2017; and references therein). Therefore, such percentage is expected to be found elsewhere. Indeed, computation of AEF measurements in the Antarctic region result in the same percentages (Burns et al., 2012). However, as explained in section 4.1, AEF measurements in continental areas can be affected by local effects as the 'Austausch' process. From Figure 9, increases of AEF is observed after sunrise, confirming global and local contributions on the AEF. It is worth to mention that for all stations daytime conditions corresponds to the period ~12-24 UT and this is the reason why the shape is very similar between the annual standard curve and the Carnegie curve. During this period of time the AEF suffers global natural increase observed in the Carnegie

curve plus the local increase due to the 'Austausch' process and local pollution (SPA and HYO station). At other places, this local increases should be at different times. For instance, Yaniv et al. (2017) showed an increase of AEF between 3-15 UT which correspond to daytime conditions for the stations they analyzed. The curves they found are different in shape with the Carnegie curve and the increase of the AEF was associated to the 'Austausch' process.

Figure 10 shows the average of the annual standard curves for all stations, called AFINSA (black) compared with the Carnegie curve (red) and EACF[2] curve (blue), in percent of the mean. Figure 10 reveals the good match between the EACF and Carnegie curve, with some differences in shape maybe related to the choice of fair weather days for EACF curve. As it is expected from Figure 9, the relative amplitude for the AFINSA curve is larger due to the 'Austausch' process. As pointed out by Kasemir (1972), the 'Austausch' process is reduced at the poles.



[2] The EACF station is located in the Brazilian station 'Estação Antarctica Comandante Ferraz' (Lat. 62.08°, Long. 58.39°, Height: 57.53 m). The EACF curve was calculated with the average of 120 days (2013: 5 days, 2014: 10 days and 2015: 115 days), which was considered only AEF positive values.

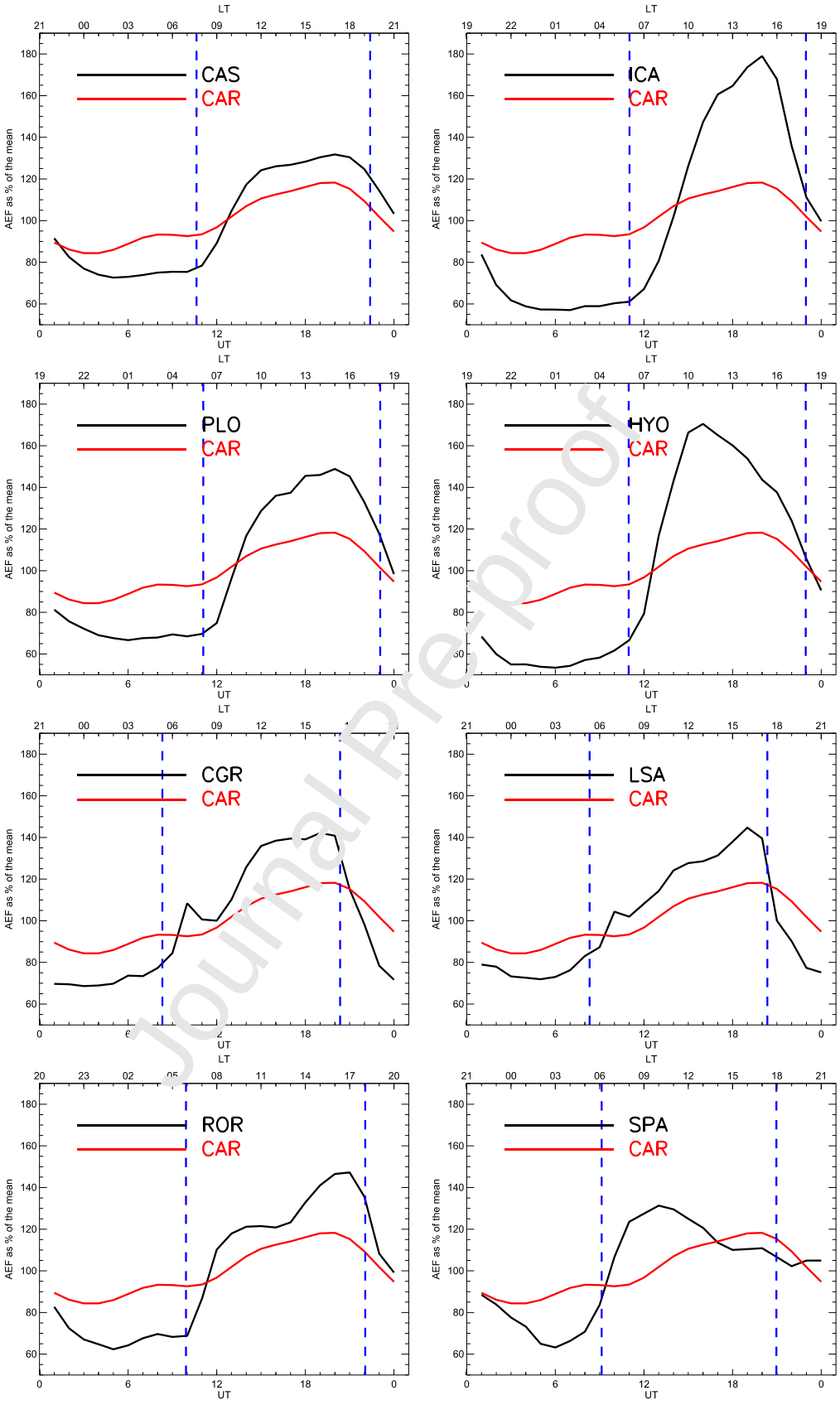

Figure 9. Annual standard curve, plotted as a percent of the mean, for all stations of AFINSA network (black curve) compared with the Carnegie curve (red curve).

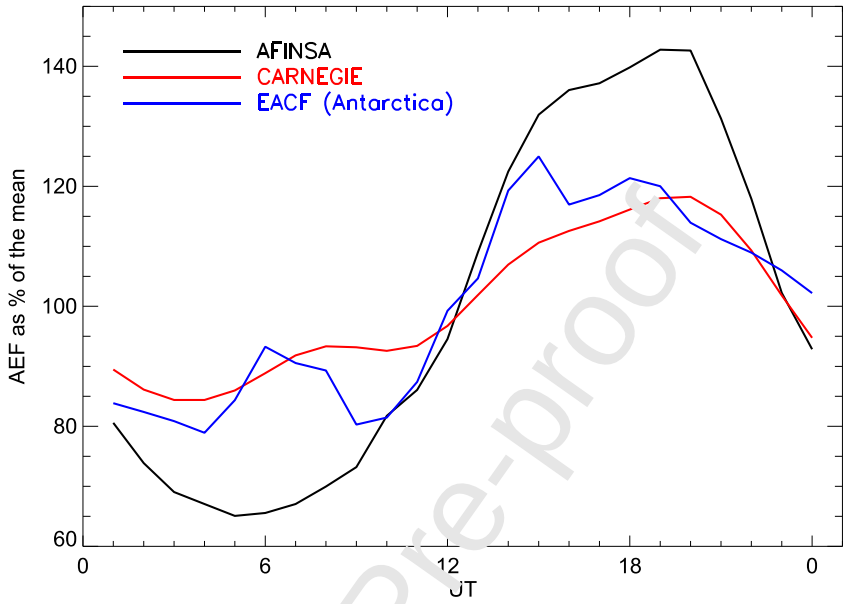


Figure 10. AFINSA standard curve (black curve), plotted as a percent of the mean, compared with the Carnegie curve (red curve) and EACF curve (blue curve).

## 5. Summary

In this paper we have presented a network of electric field mills to monitor the atmospheric electric field in South America called AFINSA. The results show the possibility of providing reliable diurnal variation curves of the AEF in fair weather conditions. There is a high correlation between the monthly standard curves for most of the stations and this is in support of a contribution of the global electric circuit in our measurements. This global contribution was also observed in the comparison with the "universal" Carnegie curve, $r \geq 0.9$ for most stations. However, it was also found a local contribution to the AEF due to the 'Austausch'

process and pollution. Such results will be important to assess how the properties of the global electric circuit vary as a function of time on different scales. From AFINSA network, data measured at CAS station is considered the best to monitor the behavior of the global electric circuit due to its local conditions, while the one at SPA station appears to be a useful proxy of anthropogenic pollution measurements in big cities. The identification of global and local effects will be important to study the behavior of the global circuit in relation to different solar and geophysical phenomena.

**Declaration of interests**

The authors declare that they have no known competing financial interests or personal relationships that could have appeared to influence the work reported in this paper.



**Acknowledgements**

JT and JPR would like to thank funding agencies CNPq (Project 422253/2016-2), CNPq (Project 312066/2016-3), CAPES (Project 88881.310386/2018-01). JT thanks the PNPD/CAPES for funding. EC thanks the National Council for Research and Development (CNPq) for individual research support (process nos: 406690/2013-8, and 303299/2016-9). The authors thank to the Geophysical Institute of Peru for the meteorological data from its Laboratory of Atmospheric Microphysics and Radiation (LAMAR-IGP). This work is partially based on data acquired at Complejo Astronómico El Leoncito, operated under agreement between the Consejo Nacional de Investigaciones Científicas y Técnicas de la República de Argentina and the National Universities of La Plata, Córdoba and San Juan. The

authors thank the reviewers for their constructive comments and suggestions, which helped to improve the quality of the paper.

**References**

Anderson, R.V., Trent, E.M., 1969. Atmospheric electricity measurements at five locations in Eastern North America. Journal of Applied Meteorology, 8, 4, 707-711.

Anisimov, S.V., Galichenko, S.V., Aphinogenov, K.V., Prokhorchuk, A.A., 2018. Evaluation of the atmospheric boundary-layer electrical variability. Boundary-Layer Meteorology, 167(2), 327-348.

Aplin, K.L., 2012. Smoke emissions from industrial western Scotland in 1859 inferred from Lord Kelvin's atmospheric electricity measurements. Atmospheric Environment, 50, 373-376.

Barthendu, 1971. Correlations of electric potential gradients at land stations and their implication on the classical picture of atmospheric electricity. Pure and Applied Geophysics, 84, 1, 13-26.

Bennett, A.J., Harrison, R.G., 2007. Atmospheric electricity in different weather conditions. Weather, 60,10, 277-283.

Burns, G.B., Frank-Kamenetsky A.V., Troshichev, O.A., Bering, E.A, Reddell, B.D., 2005. Interannual consistency of bi-monthly differences in diurnal variations of the ground-level, vertical electric field. Journal of Geophysical Research, 110, D10106.

Burns, G.B., Tinsley, B.A., Frank-Kamenetsky, A.V., Troshichev, O.A., French, W.J.R., Klekociuk, A.R., 2012. Monthly diurnal global atmospheric circuit estimates derived from Vostok electric field measurements adjusted for local meteorological and solar wind influences. Journal of the Atmospheric Sciences, 69, 6, 2061-2082.

Burns, G.B., Frank-Kamenetsky, A.V., Tinsley, B.A., French, W.J.R., Grigioni, P., Camporeale, G., Bering, E.A., 2017. Atmospheric global circuit variations from Vostok and Concordia electric field measurements. Journal of the Atmospheric Sciences, 74, 3, 783-800.

Chubb, J., 2014. The measurement of atmospheric electric fields using pole mounted electrostatic fieldmeters. Journal of Electrostatics, 72, 295-300.

Cobb, W.E., 1968. The atmospheric electric climate at Mauna Loa Observatory, Hawaii. Journal of the Atmospheric Sciences, 25, 470-480.

De, S.S., Paul, S., Barui, S., Pal, P., Bandyopadhyay, B., Kala, D., Ghosh, A., 2013. Studies on the seasonal variation of atmospheric electricity parameters at a tropical station in Kolkata, India. Journal of Atmospheric and Solar-Terrestrial Physics, 105-106, 135-141.

Gurmani, S.F., Ahmad, N., Tacza, J., Iqbal, T., 2018. First seasonal and annual variations of atmospheric electric field at a subtropical station in Islamabad, Pakistan. Journal of Atmospheric and Solar-Terrestrial Physics, 179, 441-449.

Haldoupis, C., Rycroft, M., Williams, E., Price, C., 2017. Is the "Earth-ionosphere capacitor" a valid component in the atmospheric electric circuit? Journal of Atmospheric and Solar-Terrestrial Physics, 164, 127-131.

Harrison R.G., Aplin, K.L., 2002. Mid-nineteenth century smoke concentrations near London. Atmospheric Environment 36, 4037-4043.

Harrison, R.G., 2006. Urban smoke concentrations at Kew, London, 1898 – 2004. Atmospheric Environment 40, 3327-3332.

Harrison, R.G., 2013. The Carnegie Curve. Surveys in Geophysics, 34, 2, 209-232.

Harrison, R.G., Nicoll, K.A., 2018: Fair weather criteria for atmospheric electricity measurements. Journal of Atmospheric and Solar-Terrestrial Physics, 179, 239-250.

Imyanitov, I.M., 1957. Pribory i metody dlya izucheniya elektrichestva atmosfery (Instruments and methods for studying the electricity of the atmosphere). Moscow, Gostekhizdat.

Israël, H., 1959. Atmospheric electrical agitation. Quarterly Journal of the Royal Meteorological Society, 85 (364), 91-104.

Israël, H., 1970. Atmospheric Electricity: Atmosphèarische Elektrizitèat. Available from the Israel Program for Scientific Translations vol.29 US Dept. of Commerce, National Technical Information Service, Springfield, Va., Jerusalem.

Jeeva, K., Gurubaran, S., Williams, E.R., Kamra, A.K., Sirna, A.K., Guha, A., Selvaraj, C., Nair, K.U., Dhar, A., 2016. Anomalous diurnal variation of atmospheric potential gradient and air-Earth current density observed at Maitri, Antarctica. Journal of Geophysical Research: Atmospheres, 121, 1-19.

Kamogawa, M., Suzuki, Y., Sakai, R., Fujiwara, H., Tori, T., Kakinami, Y., Watanabe, Y., Sato, R., Hashimoto, S., Okochi, H., Miura, K., Yasuda, H., Orihara, Y., Suzuki, T., 2015. Diurnal variation of atmospheric electric field at the summit of Mount Fuji, Japan, distinctly from the Carnegie curve in summertime. Geophysical Research Letter, 42, 3019-3023.

Kamra, A.K., Deshpande, C.G., Gopalakrishnan, V., 1994. Challenge to the assumption of the unitary diurnal variation of the atmospheric electric field based on observations in the Indian Ocean, Bay of Bengal and Arabian Sea. Journal of Geophysical Research, 99, N° D10, 21,043-21,050.

Kamsali, N, Pawar, S.D., Murugavel, P., Gopalakrishnan, 2011. Estimation of small ion concentration near the Earth's surface. Journal of Atmospheric and Solar-Terrestrial Physics, 73, 2345-2351.

Kasemir, H.W., 1972. Atmospheric electric measurements in the Arctic and the Antarctic. Pure and Applied Geophysics, 100, 1, 70-80.

Kubicki, M., Odzimek, A., Neska, M., Berlinski, J., Michnowski, S., 2016. First measurements of the Earth's electric field at the Arctowski Antarctic Station, King George Island, by the new Polish atmospheric electricity observation network. Acta Geophysica, 64, 6, 2630-2649.

Liu, C. Williams, E., Zipser, E.J., Burns, G., 2010. Diurnal variations of global thunderstorms and electrified shower clouds and their contribution to the global electric circuit. Journal of the Atmospheric Sciences, 67 (2), 309-323.

Lopes, F.M., Silva, H.G., Bennett, A.J., Reis, A.H., 2017. Global electric circuit research at Graciosa Island (ENA-ARM Facility): First years of measurements and ENSO influences. Journal of Electrostatics, 87, 203-211.

Lucas, G.M., Thayer, J.P., Deierling, W., 2017. Statistical analysis of spatial and temporal variations in atmospheric electric fields from a regional array of field mills. Journal of Geophysical Research: Atmospheres, 122, 1158-1174.

MacGorman, D.R., Rust, W.D., 1998. The electrical nature of storm. Oxford University Press New York, 422p.

Mach, D.A., Blakeslee, J., Bateman, M., 2011. Global electric circuit implications of combined aircraft storm electric current measurements and satellite-based diurnal lightning statistics. Journal of Geophysical Research, 116, D05201.

Manohar, G.K., Sholapurkar, S.M., Kandalgaonkar, S.S., 1990. Off-shore sea surface electric field investigations around the Indian Sub-continent during 9-20 May 1983. Advances in Atmospheric Sciences, 7, 4, 453-462.

Marshall, T.C., Rust, W.D., Stolzenburg, M., Roeder, W.P., Krehbiel, P.R., 1999. A study of enhanced fair-weather electric fields occurring soon after sunrise. Journal of Geophysical Research, 104, D20, 24455-24469.

Morita, Y., 1971. The diurnal and latitudinal variation of electric field and electric conductivity in the atmosphere over the Pacific Ocean. Journal of the Meteorological Society of Japan, 49, 1, 56-58.

Nicoll, K.A., Harrison, R.G., 2014. Detection of lower tropospheric responses to solar energetic particles at midlatitudes. Physical Review Letters, 112(22), 225001, 1-5.

Nicoll, K.A., Harrison, R.G., Silva, H.G., Salgado, R., Melgão, M., Bortoli, D., 2018. Electrical sensing of the dynamical structure of the planetary boundary layer. Atmospheric Research, 202, 81-95.

Nicoll, K.A., Harrison, R.G., Barta, V., Bor, J., Brugge, R., Chillingarian, A., Chum, J., Georgoulias, A.K., Guha, A., Kourtidis, K., Kubicki, M., Mareev, E., Matthews, J., Mkrtchyan, H., Odzimek, A., Raulin, J.-P., Robert, D., Silva, H.G., Tacza, J., Yair, Y., Yaniv, R., 2019. A global atmospheric electricity monitoring network for climate and geophysical research. Journal of Atmospheric and Solar-Terrestrial Physics, 184, 18-29.

Peterson, M., Deierling, W., Liu, Ch., Mach, D., Kalb, Ch., 2017. A TRMM/GPM retrieval of the total generator current for the global electric circuit. Journal of Geophysical Research: Atmospheres, 122, 10025-10039.

Reddell, B.D., Benbrook, J.R., Bering E.A., Cleary, E.N., Few, A.A., 2004. Seasonal variations of atmospheric electricity measured at Amundsen-Scott South Pole station. Journal of Geophysical Research, 109, A09308.

Rycroft, M.J., Nicoll, K.A, Aplin, K.L., Harrison, R.G., 2012. Recent advances in global electric circuit between the space environment and the troposphere. Journal of Atmospheric and Solar-Terrestrial Physics, 90-91, 198-211.

Saavedra, M., Takahashi, K., 2017. Physical controls on frost events in the central Andes of Peru using in situ observations and energy flux models. Agricultural and Forest Meteorology, 239, 58-70.

Saavedra, M., Junquas, C., Espinoza, J.C., Silva, Y., 2020. Impacts of topography and land use changes on the air surface temperature and precipitation over the central Peruvian Andes. Atmospheric Research, 234, 104711.

Secker, P.E., 1975. The design of simple instrumentation for measurement of charge on insulating surfaces. Journal of Electrostatics, 1 (1), 27-36.

Silva, H.G., Conceição, R., Melgão, M., Nicoll, K., Mendes, P.B., Tlemçani, M., Reis, A.H., Harrison, R.G., 2014. Atmospheric electric field measurements in urban environment and the pollutant aerosol weekly dependence. Environment Research Letters, 9, 114025.

Smirnov, S.E., Mikhailova, G.A., Kapustina, O.V., 2012. Problem of the nature of the sunrise effect in diurnal variations in the electric field in Kamchatka: 1. Time variations in the electric field. Geomagnetism and Aeronomy, 52, 4, 507-5012.

Tacza, J., Raulin, J.-P., Macotela, E., Norabuena, E., Fernandez, G., Correia, E., Rycroft, M.J., Harrison, R.G., 2014. A new South American network to study the atmospheric electric field and its variations related to geophysical phenomena. Journal of Atmospheric and Solar-Terrestrial Physics, 120, 70-79.

Tacza, J., Raulin, J.-P., Macotela, E.L., Norabuena, E.O., Fernandez, G., 2016. Atmospheric electric field variations and lower ionosphere disturbance during the total solar eclipse of 2010 July 11. Advances in Space Research, 58, 2052-2056.

Tacza, J. Raulin, J.-R., Mendonca, R.R.S., Makhmutov, V.S., Marun, A., Fernandez, G., 2018. Solar effects on the atmospheric electric field during 2010-2015 at low latitudes. Journal of Geophysical Research: Atmospheres, 123, 1-10.

Takagi, M., Kanada, M., 1972. Global variation in the atmospheric electric field. Pure and Applied Geophysics, 100, 1, 44-53.

Torreson, O.W., Parkinson, W.C., Gish, O.H., Wait, G.R., 1946. Ocean atmospheric-electric results (Scientific Results of Cruise VII of the Carnegie during 1928-1929 under command of

Captain J.P. Ault, vol3). Researches of the Department of Terrestrial Magnetism. Carnegie Institution of Washington Publication, 568.

Torreson, O.W., Wait, G.R., 1948. Atmospheric-electric results from Huancayo Observatory, Peru, 1924-1934. Researches of the Department of Terrestrial Magnetism. Carnegie Institution of Washington Publication, 175 (19), 1-547.

Tuomi, T.J., 1989. Ten year summary 1977-1986 of atmospheric electricity measured at Helsinki-Vantaa Airport, Finland. Geophysica, 25, 1&2, 1-20.

Wilson, C.T.R., 1903. Atmospheric electricity, Nature, 68, 101-104.

Wilson, C.T.R., 1921. Investigations on lightning discharges and on the electric field of thunderstorms. Philos.Trans. Roy. Soc. London, 221A, 73-115.

Whipple, F.J.W., 1929. On the association of the diurnal variation of electric potential gradient in fine weather with the distribution of thunderstorms over the globe. Quarterly Journal of the Royal Meteorological Society, 55, 1-17.

Whipple, F.J.W., 1937. The electrical characterization of days – The practice of the British Meteorological Office. Terrestrial Magnetism and Atmospheric Electricity, 42 (2), 129-136.

Williams, E.R., 2009. The global electric circuit: A review. Atmospheric Research, 91, 140-152.

Williams, E., Mareev, E., 2014. Recent progress on the global electric circuit. Atmospheric Research, 135-136, 208-227.

Xu, B., Huang, Ch., Chen, B., 2013. Observation of the variations of the atmospheric electric field at YBJ, Tibet. Meteorology and Atmospheric Physics, 21, 1-2, 99-107.

Yaniv, R., Yair, Y., Price C., Katz, S., 2016. Local and global impacts on the fair-weather electric field in Israel. Atmospheric Research, 172-173, 119-125.

Yaniv, R., Yair, Y., Price C., Mkrtchyan, H., Lynn, B., Reymers, A., 2017. Ground-based measurements of the vertical E-field in mountainous regions and the "Austausch" effect. Atmospheric Research, 189, 127-133.

Table 1. Description of the EFM sensor stations of the AFINSA network.

| ID | Lat. (°) | Long. (°) | Alt. (m) | Description |
|---|---|---|---|---|
| CAS | -31,800 | -69,293 | 2480 | Two sensors separated ~400 meters (CAS1 and CAS2) installed in 2008 and 2010, respectively. This paper contains only results for CAS2. The sensors are installed at the Complejo Astronómico El Leoncito. This place is located far from the city and is characterized by a clear sky observed most of the time during a year. The sensors are located away of housing, surrounded by scrub and low bushes. The data period used in this paper is between January 2010 - December 2018. |
| ICA | -14,089 | -75,736 | 402 | First light in 12/2011. ICA station is located at the San Luis Gonzaga University campus. The site is located in the desert coast of southern Peru, in the suburbs of Ica city. This place is characterized with a daily sunshine duration of 7 hours, average temperature of 21 °C and annual precipitation of almost zero. The clearest part of the year in Ica begins around April with a duration of ~6.2 months. The cloudiest part of the year begins around October with a duration of ~5.8 months. The data period used in this paper is between December 2011 - December 2018. However, during August 2013 - February 2014, September 2014 - June 2015, September 2015 - January 2016 and December 2016 - January 2018 there are no data for technical problems. |
| PLO | -12,504 | -76,798 | 85 | First light in 11/2011. The sensor is positioned on the roof of a house, 220 meters away from the sea |

| | | | | |
|---|---|---|---|---|
| | | | | and 1.7 km from the nearest town. No vegetation nearby. PLO station is located around 50 km from Lima city. The data period used in this paper is between November 2011 - February 2018. However, during February 2013 - October 2014 and May 2017 - December 2017, there are no data for technical problems. |
| ROR | 2,87 | -60,71 | 78 | First light in 04/2014. The sensor is positioned at an altitude of 1.6 meters. ROR station is located 18 km from Boa Vista city, in a region dominated by the Amazonian savannah. This place is characterized by a rainy season (April to August) where the average humidity is 90% while the months from October to February have clear skies with average humidity around 65%. Annual average temperature between 28ºC and 36ºC. The data period used in this paper is between April 2014 - December 2018. However, during June 2014 - April 2015 and December 2017 - February 2018, there are no data for technical problems. |
| HYO | -12,04 | -75,32 | 3350 | First light in 06/2016. The sensor is positioned 50 cm from the ground, 15 m from a house. The nearest town is 3.5 km. HYO station is located about 15 km from Huancayo city. The data period used in this paper is between June 2016 - December 2018. However, during January 2017 – March 2018, there are no data for technical problems. |
| CGR | -7,21 | -35,91 | 550 | First light in 11/2016. The sensor is installed on the roof of a building in the State University of |

| | | | | |
|---|---|---|---|---|
| | | | | Paraíba, located in the center of the Campina Grande city. The data period used in this paper is between November 2016 - December 2018. |
| LSA | -7,16 | -35,87 | 630 | First light in 05/2017. The sensor is installed on the roof of a house. LSA station is located ~8 km of CGR station. The data period used in this paper is between May 2017 - December 2018. |
| SPA | -23,55 | -46,65 | 810 | First light in 04/2017. The sensor is installed on the roof of a building at Mackenzie Presbyterian University in São Paulo city. The data period used in this paper is between April 2017 - December 2018. |

Table 2. Total number of 'fair weather' days for each station using the observational criterion for each month. '()' indicates the average of 'fair weather' days for each month.

| Month | CAS | ROR | CGR | LSA | ICA | PLO | HYO | SPA |
|---|---|---|---|---|---|---|---|---|
| January | 103 (11) | 13 (6) | 0 | 0 | 8 (3) | 109 (21) | - | 7 (7) |
| February | 109 (12) | 15 (15) | 0 | 0 | 24 (7) | 65 (20) | - | 19 (19) |
| March | 204 (23) | 21 (7) | 0 | 0 | 19 (6) | 67 (17) | - | 7 (7) |
| April | 187 (23) | 19 (6) | 14 (7) | 5 (5) | 28 (9) | 3[illegible] (19) | 3 (2) | 31 (16) |
| May | 193 (24) | 24 (6) | 28 (14) | 16 (8) | 57 (14) | 77 (20) | 18 (18) | 31 (16) |
| June | 182 (23) | 2 (1) | 21 (11) | 11 (6) | [illegible]0 (15) | 34 (17) | 27 (27) | 22 (11) |
| July | 185 (22) | 6 (2) | 23 (12) | 2[illegible] (11) | 81 (20) | 22 (8) | 42 (21) | 15 (8) |
| August | 185 (21) | 19 (8) | 21 (11) | 14 (7) | 60 (12) | 25 (12) | 14 (7) | 25 (13) |
| September | 183 (23) | 33 (8) | 15 (8) | 7 (4) | 35 (9) | 29 (10) | 20 (10) | 20 (10) |
| October | 159 (20) | 19 (6) | 0 | 0 | 22 (11) | 76 (19) | 6 (3) | 22 (11) |
| November | 157 (20) | 47 (15) | 0 | 0 | 16 (8) | 67 (17) | 8 (4) | 24 (12) |

| | | | | | | | | |
|---|---|---|---|---|---|---|---|---|
| December | 123 (15) | 22 (7) | 0 | 0 | 31 (8) | 69 (13) | 2 (2) | 19 (10) |
| Total | 1970 | 240 | 143 | 74 | 441 | 679 | 140 | 242 |

Table 3. Linear correlation coefficient between all stations of AFINSA network by month.

| | CAS | ROR | CGR | LSA | ICA | PLO | HYO | SPA | | CAS | ROR | CGR | LSA | ICA | PLO | HYO | SPA |
|---|---|---|---|---|---|---|---|---|---|---|---|---|---|---|---|---|---|
| | **JANUARY** | | | | | | | | | **FEBRUARY** | | | | | | | |
| **CAS** | 1 | 0.55 | x | x | 0.83 | 0.92 | x | 0.52 | **CAS** | 1 | 0.92 | x | x | 0.85 | 0.95 | x | 0.38 |
| **ROR** | 0.55 | 1 | x | x | 0.51 | 0.62 | x | 0.56 | **ROR** | 0.92 | 1 | x | x | 0.81 | 0.96 | x | 0.38 |
| **CGR** | x | x | x | x | x | x | x | x | **CGR** | x | x | x | x | x | x | x | x |
| **LSA** | x | x | x | x | x | x | x | x | **LSA** | x | x | x | x | x | x | x | x |
| **ICA** | 0.83 | 0.51 | x | x | 1 | 0.89 | x | 0.64 | **ICA** | 0.85 | 0.81 | x | x | 1 | 0.90 | x | 0.26 |
| **PLO** | 0.92 | 0.62 | x | x | 0.89 | 1 | x | 0.54 | **PLO** | 0.95 | 0.96 | x | x | 0.90 | 1 | x | 0.33 |
| **HYO** | x | x | x | x | x | x | x | x | **HYO** | x | x | x | x | x | x | x | x |
| **SPA** | 0.52 | 0.56 | x | x | 0.64 | 0.54 | x | 1 | **SPA** | 0.38 | 0.38 | x | x | 0.26 | 0.33 | x | 1 |
| | **MARCH** | | | | | | | | | **APRIL** | | | | | | | |
| **CAS** | 1 | 0.92 | x | x | 0.91 | 0.97 | x | 0.60 | **CAS** | 1 | 0.94 | 0.70 | 0.53 | 0.97 | 0.94 | 0.95 | 0.62 |
| **ROR** | 0.92 | 1 | x | x | 0.90 | 0.92 | x | 0.62 | **ROR** | 0.94 | 1 | 0.70 | 0.51 | 0.89 | 0.90 | 0.87 | 0.73 |
| **CGR** | x | x | x | x | x | x | x | x | **CGR** | 0.70 | 0.70 | 1 | 0.83 | 0.66 | 0.51 | 0.69 | 0.69 |
| **LSA** | x | x | x | x | x | x | x | x | **LSA** | 0.53 | 0.51 | 0.83 | 1 | 0.43 | 0.32 | 0.56 | 0.70 |

| | | | | | | | | | | | | | | | | |
|---|---|---|---|---|---|---|---|---|---|---|---|---|---|---|---|---|
| **ICA** | 0.91 | 0.90 | x | x | 1 | 0.97 | x | 0.46 | **ICA** | 0.97 | 0.89 | 0.66 | 0.43 | 1 | 0.92 | 0.94 | 0.51 |
| **PLO** | 0.97 | 0.92 | x | x | 0.97 | 1 | x | 0.53 | **PLO** | 0.94 | 0.90 | 0.51 | 0.32 | 0.92 | 1 | 0.85 | 0.49 |
| **HYO** | x | x | x | x | x | x | x | x | **HYO** | 0.95 | 0.87 | 0.69 | 0.56 | 0.94 | 0.85 | 1 | 0.63 |
| **SPA** | 0.60 | 0.62 | x | x | 0.46 | 0.53 | x | 1 | **SPA** | 0.62 | 0.73 | 0.69 | 0.70 | 0.51 | 0.49 | 0.63 | 1 |
| | | | **MAY** | | | | | | | | | | **JUNE** | | | | |
| **CAS** | 1 | 0.84 | 0.85 | 0.64 | 0.98 | 0.97 | 0.87 | 0.53 | **CAS** | 1 | 0.65 | 0.76 | 0.59 | 0.98 | 0.99 | 0.91 | 0.55 |
| **ROR** | 0.84 | 1 | 0.71 | 0.49 | 0.88 | 0.89 | 0.77 | 0.81 | **ROR** | 0.65 | 1 | 0.45 | 0.31 | 0.69 | 0.60 | 0.52 | 0.64 |
| **CGR** | 0.85 | 0.71 | 1 | 0.91 | 0.79 | 0.72 | 0.86 | 0.67 | **CGR** | 0.76 | 0.45 | 1 | 0.89 | 0.70 | 0.76 | 0.87 | 0.64 |
| **LSA** | 0.64 | 0.49 | 0.91 | 1 | 0.56 | 0.47 | 0.77 | 0.53 | **LSA** | 0.59 | 0.31 | 0.89 | 1 | 0.55 | 0.62 | 0.69 | 0.45 |
| **ICA** | 0.98 | 0.88 | 0.79 | 0.56 | 1 | 0.98 | 0.83 | 0.53 | **ICA** | 0.98 | 0.69 | 0.70 | 0.55 | 1 | 0.98 | 0.84 | 0.55 |
| **PLO** | 0.97 | 0.89 | 0.72 | 0.47 | 0.98 | 1 | 0.79 | 0.53 | **PLO** | 0.99 | 0.60 | 0.76 | 0.62 | 0.98 | 1 | 0.89 | 0.52 |
| **HYO** | 0.87 | 0.77 | 0.86 | 0.77 | 0.83 | 0.79 | 1 | 0.62 | **HYO** | 0.91 | 0.52 | 0.87 | 0.69 | 0.84 | 0.89 | 1 | 0.63 |
| **SPA** | 0.53 | 0.81 | 0.67 | 0.53 | 0.53 | 0.53 | 0.62 | 1 | **SPA** | 0.55 | 0.64 | 0.64 | 0.45 | 0.55 | 0.52 | 0.63 | 1 |

Table 3. Continue

| | CAS | ROR | CGR | LSA | ICA | PLO | HYO | SPA | | CAS | ROR | CGR | LSA | ICA | PLO | HYO | SPA |
|---|---|---|---|---|---|---|---|---|---|---|---|---|---|---|---|---|---|
| | | | | JULY | | | | | | | | | AUGUST | | | | |
| **CAS** | 1 | 0.91 | 0.84 | 0.78 | 0.96 | 0.96 | 0.90 | 0.77 | **CAS** | 1 | 0.96 | 0.66 | 0.77 | 0.94 | 0.94 | 0.83 | 0.72 |
| **ROR** | 0.91 | 1 | 0.76 | 0.68 | 0.84 | 0.78 | 0.79 | 0.85 | **ROR** | 0.96 | 1 | 0.62 | 0.75 | 0.91 | 0.84 | 0.77 | 0.80 |
| **CGR** | 0.84 | 0.76 | 1 | 0.95 | 0.86 | 0.82 | 0.90 | 0.81 | **CGR** | 0.66 | 0.62 | 1 | 0.96 | 0.56 | 0.59 | 0.86 | 0.60 |
| **LSA** | 0.78 | 0.68 | 0.95 | 1 | 0.83 | 0.80 | 0.85 | 0.66 | **LSA** | 0.77 | 0.75 | 0.96 | 1 | 0.66 | 0.68 | 0.90 | 0.70 |
| **ICA** | 0.96 | 0.84 | 0.86 | 0.83 | 1 | 0.99 | 0.93 | 0.74 | **ICA** | 0.94 | 0.91 | 0.56 | 0.66 | 1 | 0.98 | 0.72 | 0.57 |
| **PLO** | 0.96 | 0.78 | 0.82 | 0.80 | 0.99 | 1 | 0.91 | 0.65 | **PLO** | 0.94 | 0.84 | 0.59 | 0.68 | 0.98 | 1 | 0.78 | 0.54 |
| **HYO** | 0.90 | 0.79 | 0.90 | 0.85 | 0.93 | 0.91 | 1 | 0.79 | **HYO** | 0.83 | 0.77 | 0.86 | 0.90 | 0.72 | 0.78 | 1 | 0.68 |
| **SPA** | 0.77 | 0.85 | 0.81 | 0.66 | 0.74 | 0.65 | 0.79 | 1 | **SPA** | 0.72 | 0.80 | 0.60 | 0.70 | 0.57 | 0.54 | 0.68 | 1 |
| | | | | SEPTEMBER | | | | | | | | | OCTOBER | | | | |
| **CAS** | 1 | 0.96 | 0.92 | 0.88 | 0.89 | 0.97 | 0.98 | 0.71 | **CAS** | 1 | 0.95 | x | x | 0.89 | 0.91 | 0.95 | 0.72 |
| **ROR** | 0.96 | 1 | 0.85 | 0.87 | 0.86 | 0.94 | 0.93 | 0.78 | **ROR** | 0.95 | 1 | x | x | 0.87 | 0.88 | 0.96 | 0.80 |
| **CGR** | 0.92 | 0.85 | 1 | 0.94 | 0.82 | 0.91 | 0.92 | 0.73 | **CGR** | x | x | x | x | x | x | x | x |
| **LSA** | 0.88 | 0.87 | 0.94 | 1 | 0.77 | 0.85 | 0.86 | 0.79 | **LSA** | x | x | x | x | x | x | x | x |
| **ICA** | 0.89 | 0.86 | 0.82 | 0.77 | 1 | 0.92 | 0.84 | 0.48 | **ICA** | 0.89 | 0.87 | x | x | 1 | 0.98 | 0.87 | 0.52 |

| | | | | | | | | | | | | | | | | |
|---|---|---|---|---|---|---|---|---|---|---|---|---|---|---|---|---|
| **PLO** | 0.97 | 0.94 | 0.91 | 0.85 | 0.92 | 1 | 0.95 | 0.68 | **PLO** | 0.91 | 0.88 | x | x | 0.98 | 1 | 0.89 | 0.51 |
| **HYO** | 0.98 | 0.93 | 0.92 | 0.86 | 0.84 | 0.95 | 1 | 0.76 | **HYO** | 0.95 | 0.96 | x | x | 0.87 | 0.89 | 1 | 0.70 |
| **SPA** | 0.71 | 0.78 | 0.73 | 0.79 | 0.48 | 0.68 | 0.76 | 1 | **SPA** | 0.72 | 0.80 | x | x | 0.52 | 0.51 | 0.70 | 1 |
| | | | **NOVEMBER** | | | | | | | | | **DECEMBER** | | | | |
| **CAS** | 1 | 0.86 | x | x | 0.84 | 0.91 | 0.89 | 0.43 | **CAS** | 1 | 0.91 | x | x | 0.85 | 0.94 | 0.75 | 0.62 |
| **ROR** | 0.86 | 1 | x | x | 0.94 | 0.90 | 0.86 | 0.44 | **ROR** | 0.91 | 1 | x | x | 0.85 | 0.91 | 0.86 | 0.70 |
| **CGR** | x | x | x | x | x | x | x | x | **CGR** | x | x | x | x | x | x | x | x |
| **LSA** | x | x | x | x | x | x | x | x | **LSA** | x | x | x | x | x | x | x | x |
| **ICA** | 0.84 | 0.94 | x | x | 1 | 0.94 | 0.84 | 0.28 | **ICA** | 0.85 | 0.85 | x | x | 1 | 0.95 | 0.76 | 0.50 |
| **PLO** | 0.91 | 0.90 | x | x | 0.94 | 1 | 0.95 | 0.38 | **PLO** | 0.94 | 0.91 | x | x | 0.95 | 1 | 0.77 | 0.50 |
| **HYO** | 0.89 | 0.86 | x | x | 0.84 | 0.95 | 1 | 0.57 | **HYO** | 0.75 | 0.86 | x | x | 0.76 | 0.77 | 1 | 0.75 |
| **SPA** | 0.43 | 0.44 | x | x | 0.28 | 0.38 | 0.57 | 1 | **SPA** | 0.62 | 0.70 | x | x | 0.50 | 0.50 | 0.75 | 1 |

Table 4. Linear correlation coefficient between all stations of AFINSA network by season.

| | CAS | ROR | CGR | LSA | ICA | PLO | HYO | SPA | | CAS | ROR | CGR | LSA | ICA | PLO | HYO | SPA |
|---|---|---|---|---|---|---|---|---|---|---|---|---|---|---|---|---|---|
| | **SUMMER** | | | | | | | | | **AUTUMN** | | | | | | | |
| **CAS** | 1 | 0.87 | x | x | 0.86 | 0.94 | 0.74 | 0.52 | **CAS** | 1 | 0.94 | 0.80 | 0.61 | 0.98 | 0.99 | 0.92 | 0.63 |
| **ROR** | 0.87 | 1 | x | x | 0.81 | 0.90 | 0.87 | 0.58 | **ROR** | 0.94 | 1 | 0.76 | 0.57 | 0.91 | 0.93 | 0.83 | 0.77 |
| **CGR** | x | x | x | x | x | x | x | x | **CGR** | 0.80 | 0.76 | 1 | 0.92 | 0.78 | 0.74 | 0.85 | 0.65 |
| **LSA** | x | x | x | x | x | x | x | x | **LSA** | 0.61 | 0.57 | 0.92 | 1 | 0.57 | 0.52 | 0.76 | 0.61 |
| **ICA** | 0.86 | 0.81 | x | x | 1 | 0.95 | 0.76 | 0.43 | **ICA** | 0.98 | 0.91 | 0.78 | 0.57 | 1 | 0.98 | 0.88 | 0.53 |
| **PLO** | 0.94 | 0.90 | x | x | 0.95 | 1 | 0.80 | 0.44 | **PLO** | 0.99 | 0.93 | 0.74 | 0.52 | 0.98 | 1 | 0.86 | 0.56 |
| **HYO** | 0.74 | 0.87 | x | x | 0.76 | 0.80 | 1 | 0.69 | **HYO** | 0.63 | 0.77 | 0.65 | 0.61 | 0.53 | 0.56 | 1 | 0.63 |
| **SPA** | 0.52 | 0.58 | x | x | 0.43 | 0.44 | 0.69 | 1 | **SPA** | 0.63 | 0.77 | 0.65 | 0.61 | 0.53 | 0.56 | 0.63 | 1 |
| | **WINTER** | | | | | | | | | **SPRING** | | | | | | | |
| **CAS** | 1 | 0.94 | 0.77 | 0.76 | 0.98 | 0.97 | 0.90 | 0.69 | **CAS** | 1 | 0.95 | 0.89 | 0.75 | 0.89 | 0.95 | 0.97 | 0.63 |
| **ROR** | 0.94 | 1 | 0.70 | 0.69 | 0.92 | 0.87 | 0.82 | 0.83 | **ROR** | 0.95 | 1 | 0.91 | 0.85 | 0.90 | 0.94 | 0.93 | 0.67 |
| **CGR** | 0.77 | 0.70 | 1 | 0.98 | 0.75 | 0.76 | 0.89 | 0.71 | **CGR** | 0.89 | 0.91 | 1 | 0.92 | 0.86 | 0.93 | 0.94 | 0.67 |

| | | | | | | | | | | | | | | | | |
|---|---|---|---|---|---|---|---|---|---|---|---|---|---|---|---|---|
| **LSA** | 0.76 | 0.69 | 0.98 | 1 | 0.75 | 0.75 | 0.87 | 0.66 | **LSA** | 0.75 | 0.85 | 0.92 | 1 | 0.75 | 0.81 | 0.82 | 0.69 |
| **ICA** | 0.98 | 0.92 | 0.75 | 0.75 | 1 | 0.99 | 0.87 | 0.64 | **ICA** | 0.89 | 0.90 | 0.86 | 0.75 | 1 | 0.97 | 0.86 | 0.41 |
| **PLO** | 0.97 | 0.87 | 0.76 | 0.75 | 0.99 | 1 | 0.89 | 0.58 | **PLO** | 0.95 | 0.94 | 0.93 | 0.81 | 0.97 | 1 | 0.95 | 0.51 |
| **HYO** | 0.90 | 0.82 | 0.89 | 0.87 | 0.87 | 0.89 | 1 | 0.72 | **HYO** | 0.97 | 0.93 | 0.94 | 0.82 | 0.86 | 0.95 | 1 | 0.67 |
| **SPA** | 0.69 | 0.83 | 0.71 | 0.66 | 0.64 | 0.58 | 0.72 | 1 | **SPA** | 0.63 | 0.67 | 0.67 | 0.69 | 0.41 | 0.51 | 0.67 | 1 |

Table 5. Linear correlation coefficient between all stations of AFINSA network by year.

| ANNUAL | | | | | | | | | |
|---|---|---|---|---|---|---|---|---|---|
| | **CAS** | **ROR** | **CGR** | **LSA** | **ICA** | **PLO** | **HYO** | **SPA** | **CAR** |
| **CAS** | 1 | 0.96 | 0.80 | 0.75 | 0.96 | 0.99 | 0.96 | 0.66 | 0.95 |
| **ROR** | 0.96 | 1 | 0.81 | 0.77 | 0.91 | 0.94 | 0.91 | 0.74 | 0.95 |
| **CGR** | 0.80 | 0.81 | 1 | 0.98 | 0.80 | 0.81 | 0.90 | 0.74 | 0.90 |
| **LSA** | 0.75 | 0.77 | 0.98 | 1 | 0.75 | 0.75 | 0.85 | 0.75 | 0.86 |
| **ICA** | 0.96 | 0.91 | 0.80 | 0.75 | 1 | 0.98 | 0.91 | 0.51 | 0.94 |
| **PLO** | 0.99 | 0.94 | 0.81 | 0.75 | 0.98 | 1 | 0.95 | 0.58 | 0.96 |
| **HYO** | 0.96 | 0.91 | 0.90 | 0.85 | 0.91 | 0.95 | 1 | 0.71 | 0.95 |
| **SPA** | 0.66 | 0.74 | 0.74 | 0.75 | 0.51 | 0.58 | 0.71 | 1 | 0.66 |
| **CAR** | 0.95 | 0.95 | 0.90 | 0.86 | 0.94 | 0.96 | 0.95 | 0.66 | 1 |

**Highlights**

- A new network to monitor the atmospheric electric field on the ground.
- Global and local contribution are found in the electric field standard curves.
- Annual standard curves have a high correlation with the 'universal' Carnegie curve.

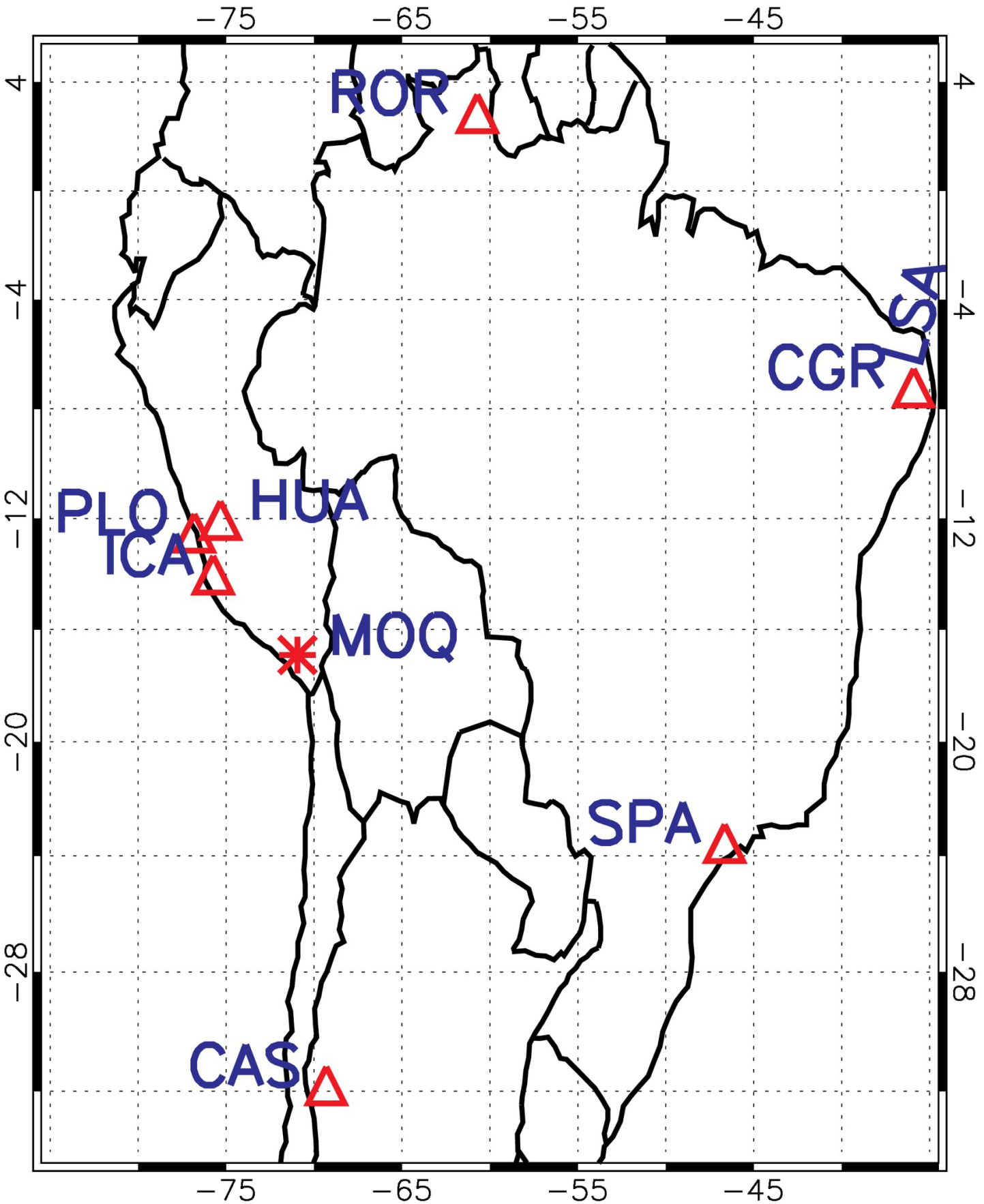


Figure 1

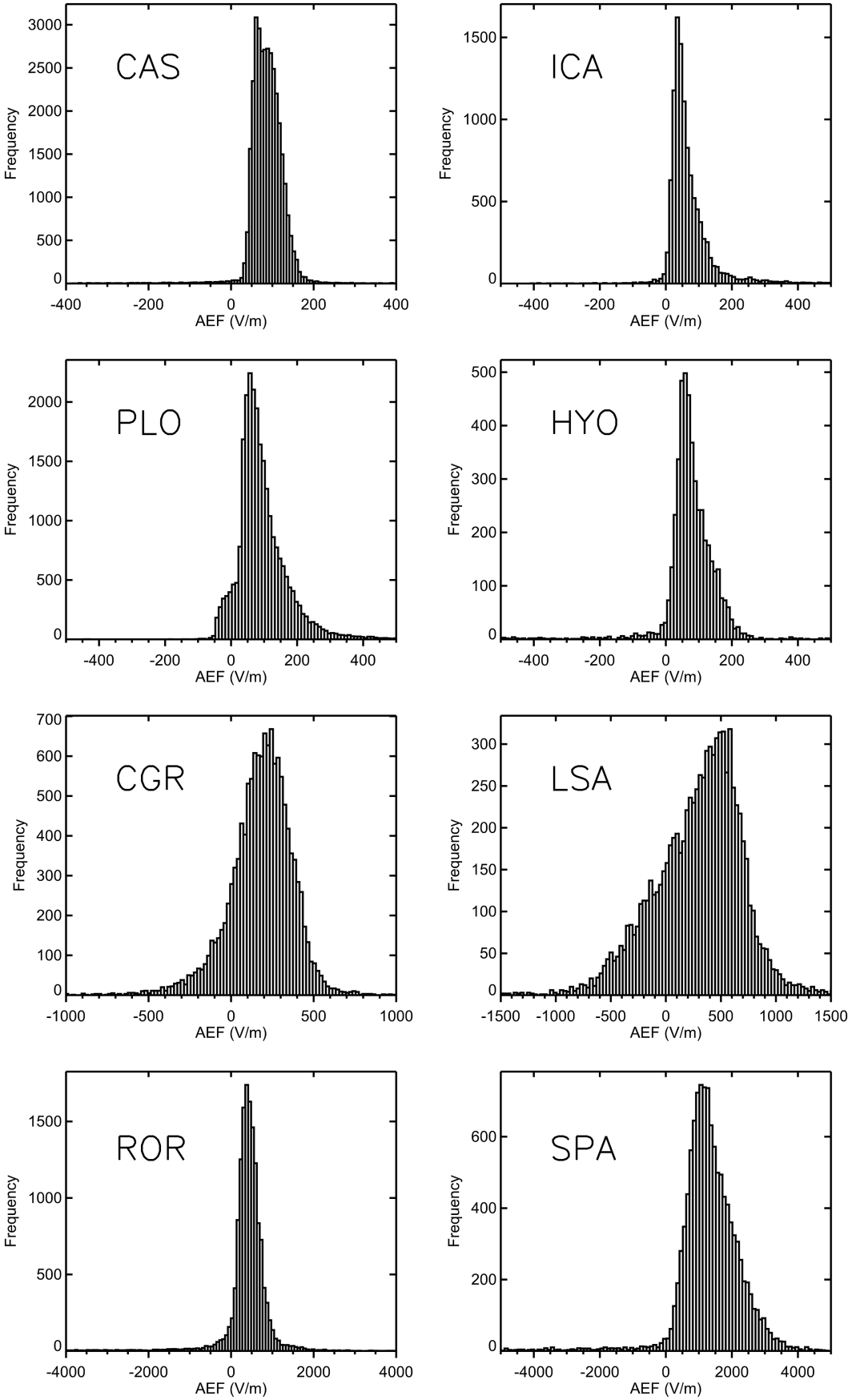
CAS
Frequency
AEF (V/m)
ICA
Frequency
AEF (V/m)
PLO
Frequency
AEF (V/m)
HYO
Frequency
AEF (V/m)
CGR
Frequency
AEF (V/m)
LSA
Frequency
AEF (V/m)
ROR
Frequency
AEF (V/m)
SPA
Frequency
AEF (V/m)

Figure 2

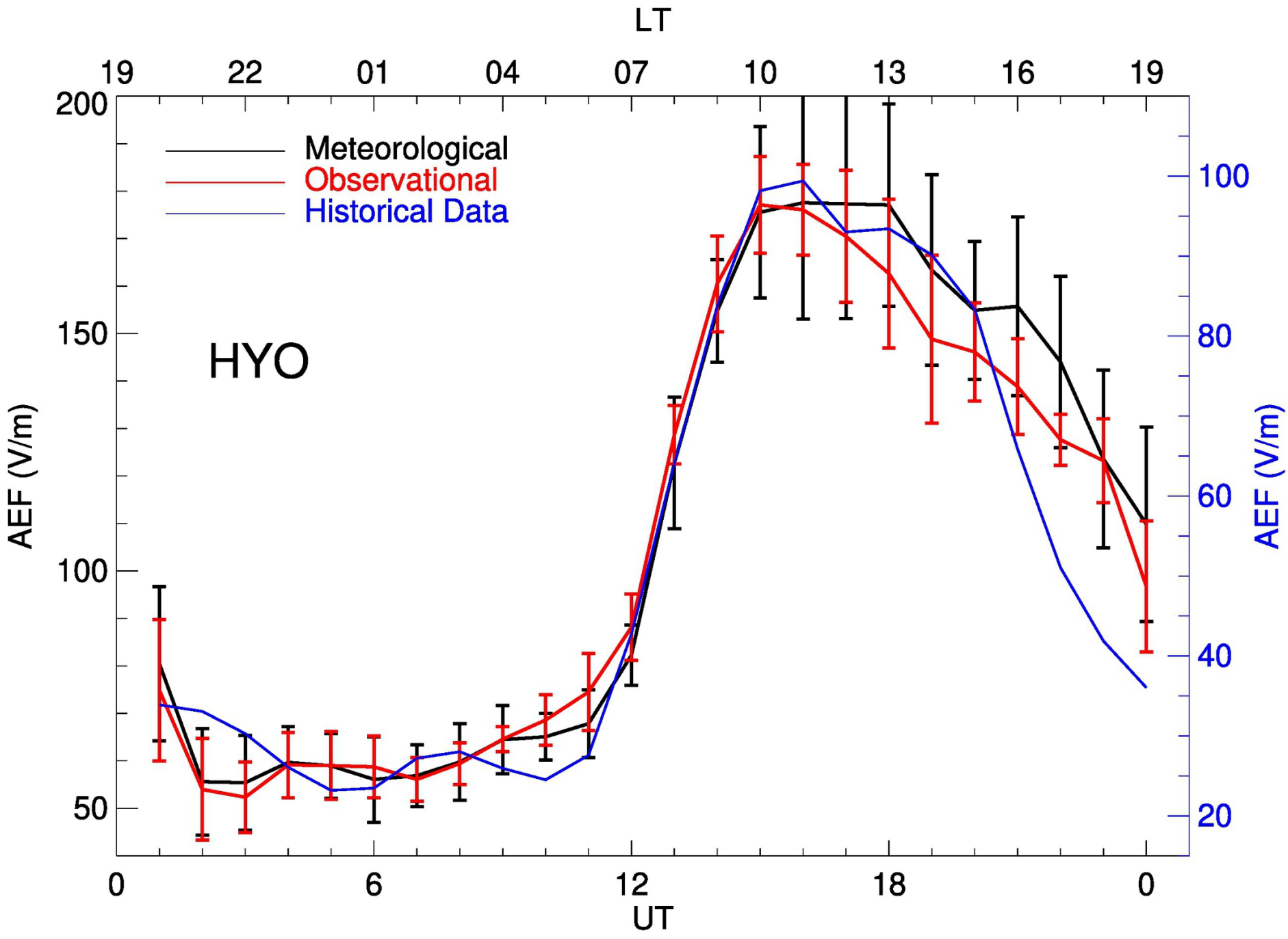
LT
19
22
01
04
07
10
13
16
19
200
150
100
50
AEF (V/m)
Meteorological
Observational
Historical Data
HYO
100
80
60
40
20
AEF (V/m)
0
6
12
18
0
UT

Figure 3

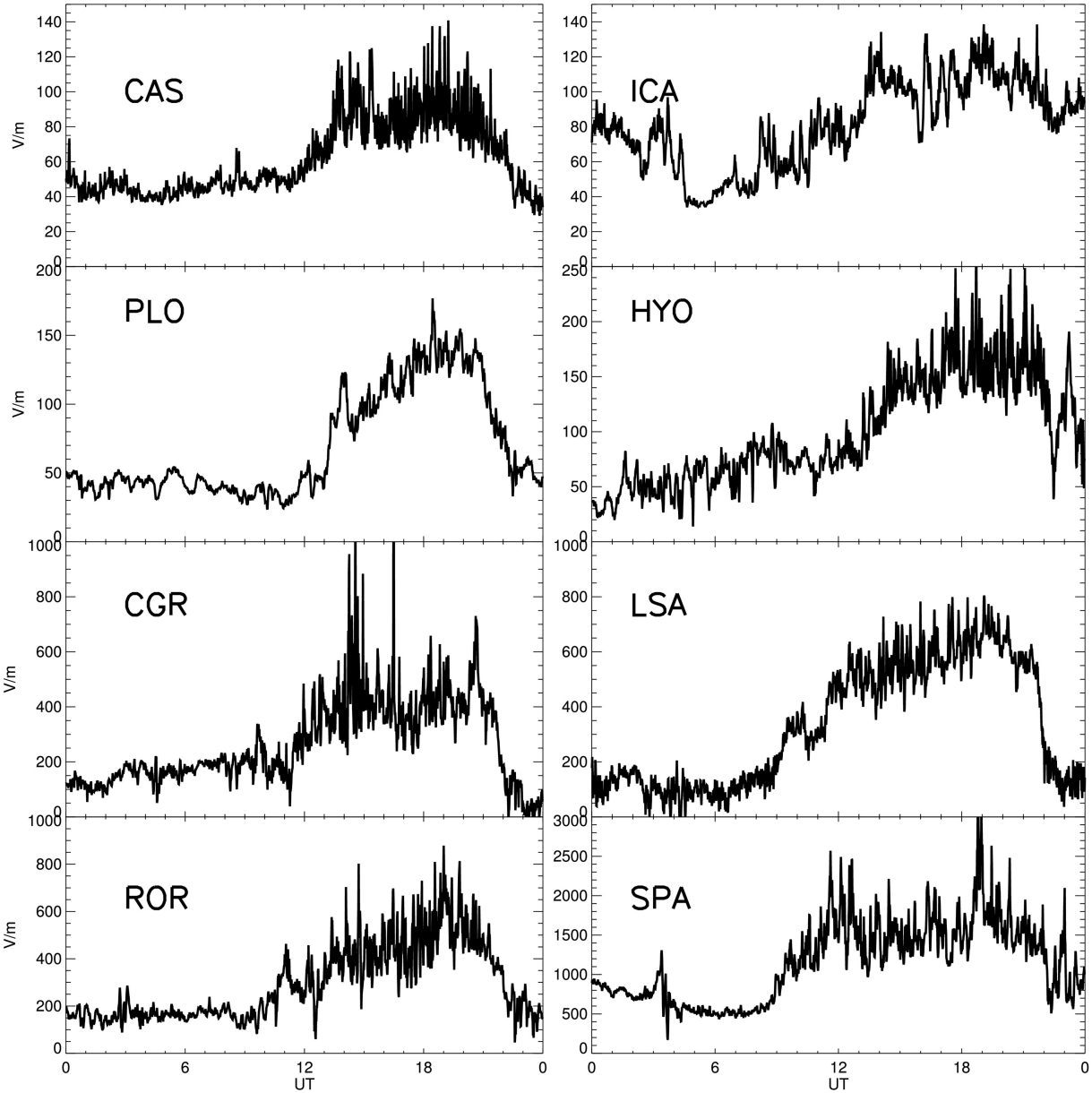


Figure 4

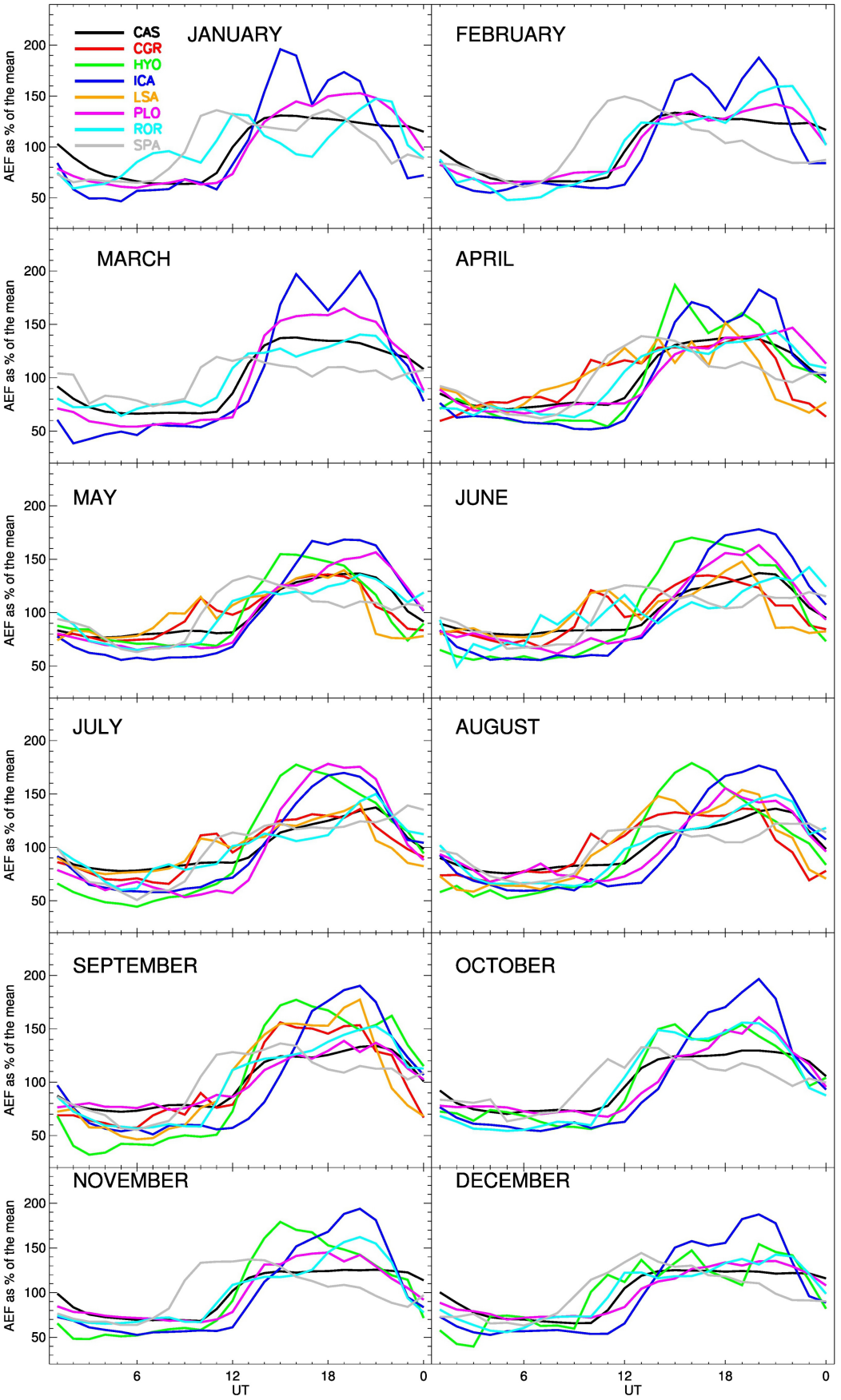
CAS
CGR
HYO
ICA
LSA
PLO
ROR
SPA
JANUARY
FEBRUARY
MARCH
APRIL
MAY
JUNE
JULY
AUGUST
SEPTEMBER
OCTOBER
NOVEMBER
DECEMBER
AEF as % of the mean
50
100
150
200
6
12
18
0
UT

Figure 5

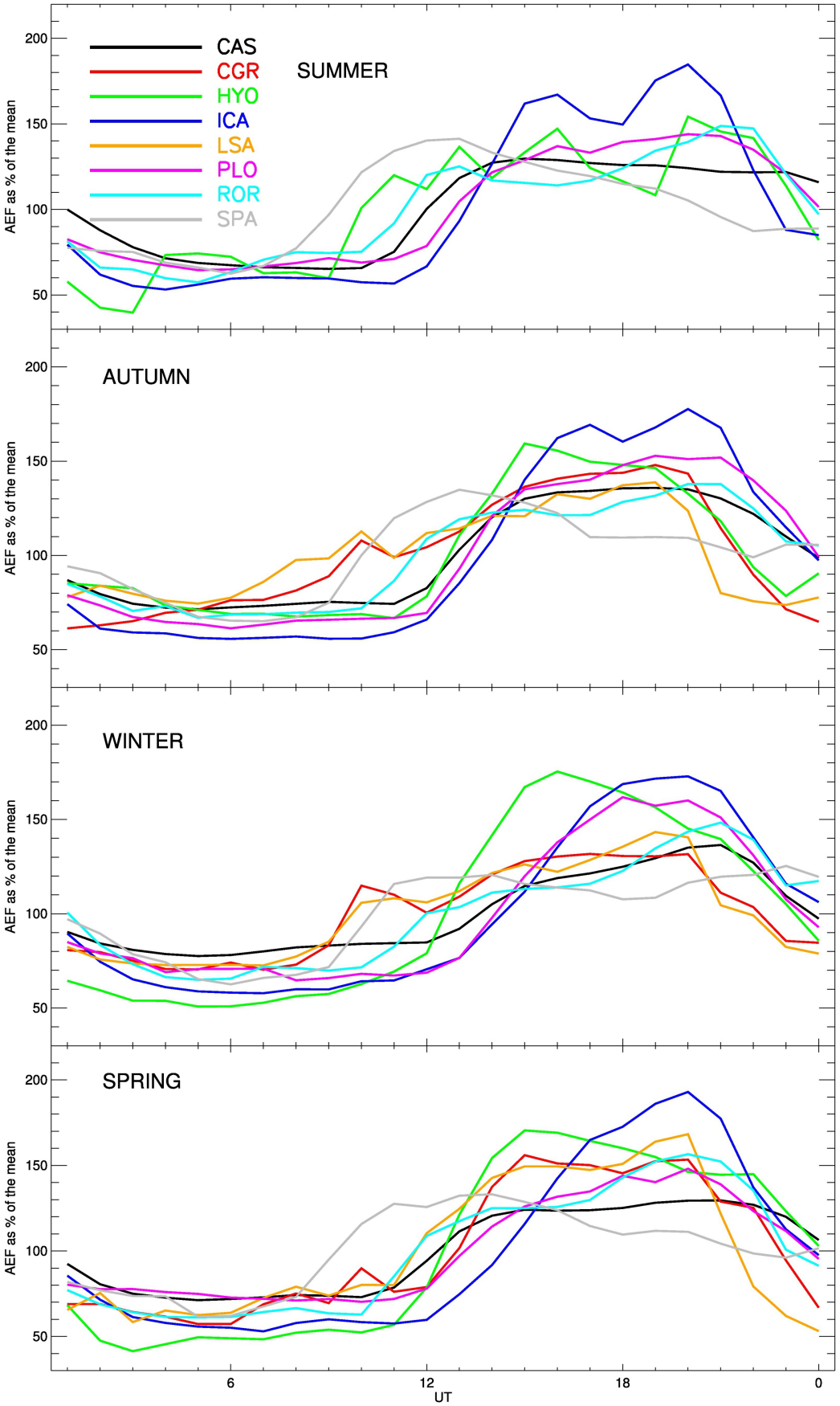
CAS
CGR
HYO
ICA
LSA
PLO
ROR
SPA
SUMMER
AUTUMN
WINTER
SPRING
AEF as % of the mean
200
150
100
50
6
12
18
0
UT

Figure 6

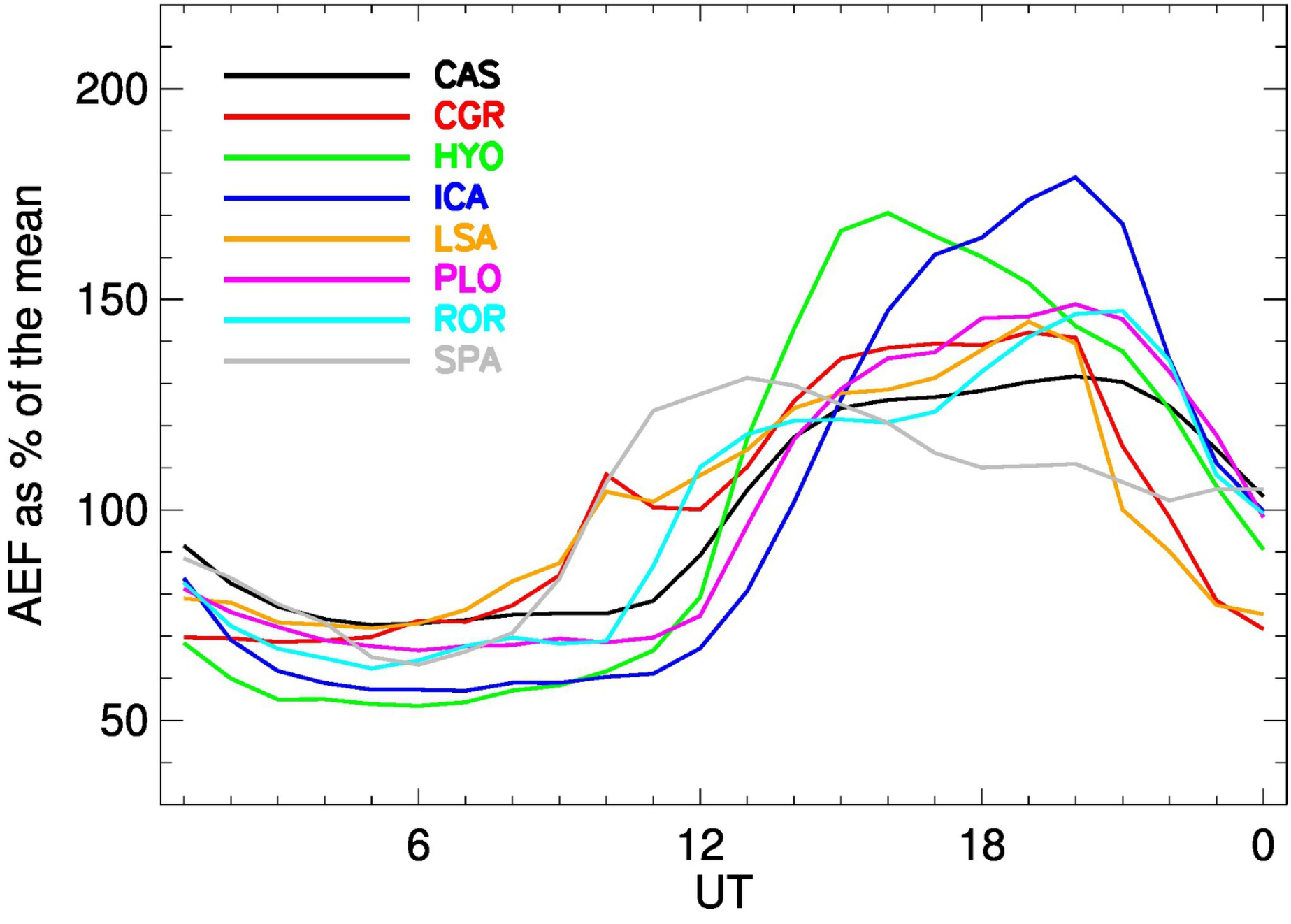
CAS
CGR
HYO
ICA
LSA
PLO
ROR
SPA
200
150
100
50
AEF as % of the mean
6
12
18
0
UT

Figure 7

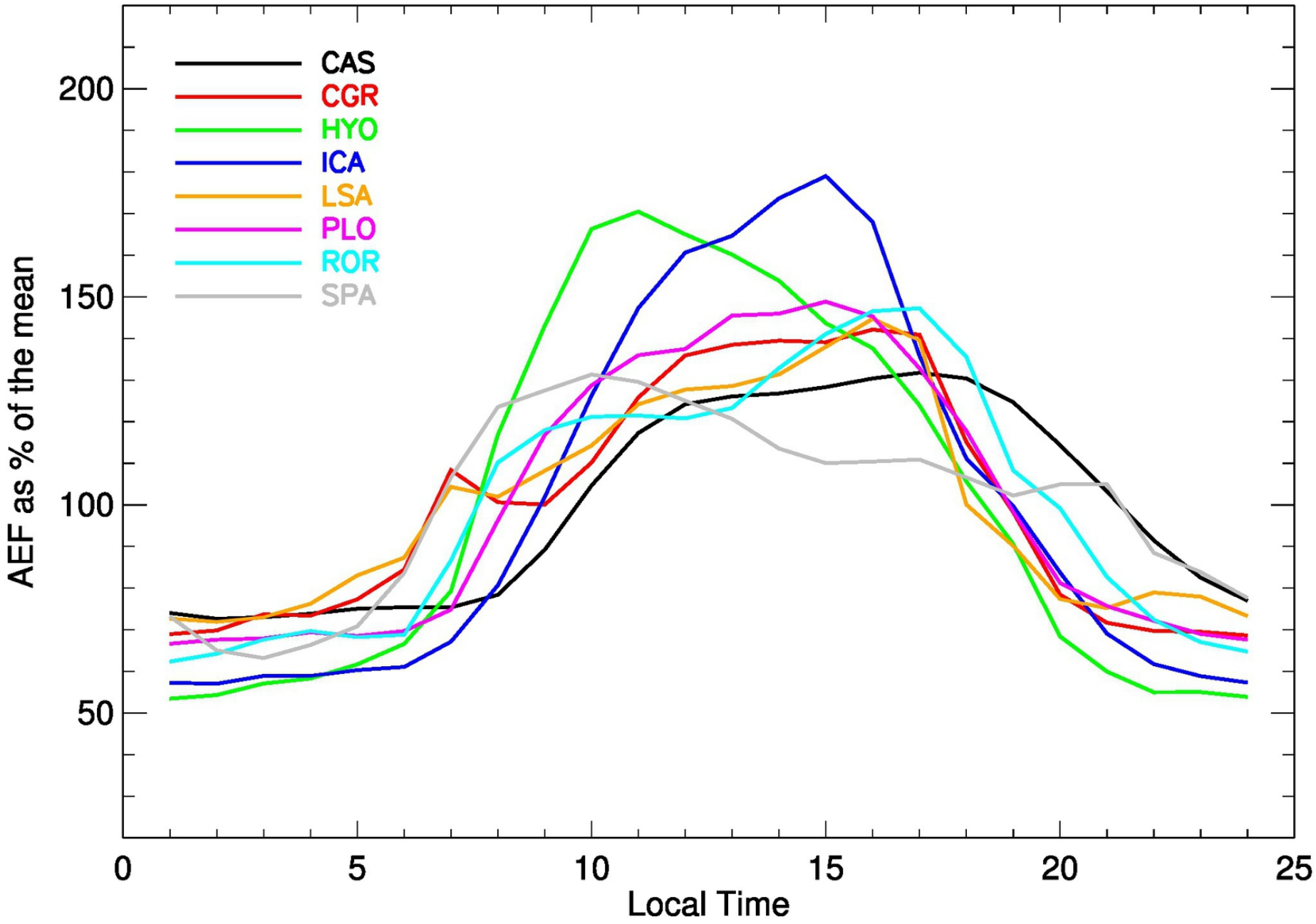
CAS
CGR
HYO
ICA
LSA
PLO
ROR
SPA
200
150
100
50
AEF as % of the mean
0
5
10
15
20
25
Local Time

Figure 8

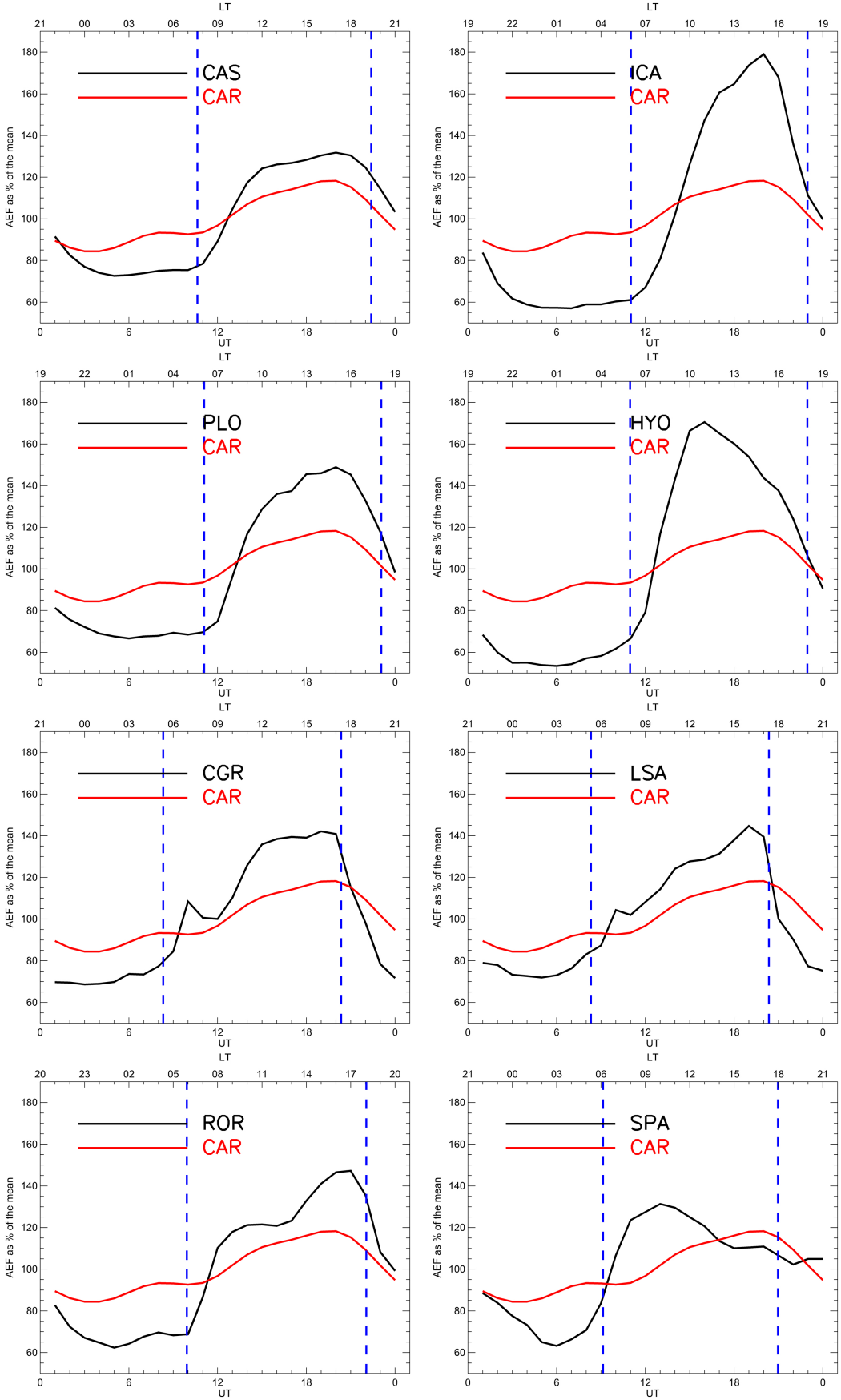
CAS
CAR
ICA
CAR
PLO
CAR
HYO
CAR
CGR
CAR
LSA
CAR
ROR
CAR
SPA
CAR
AEF as % of the mean
LT
UT

Figure 9

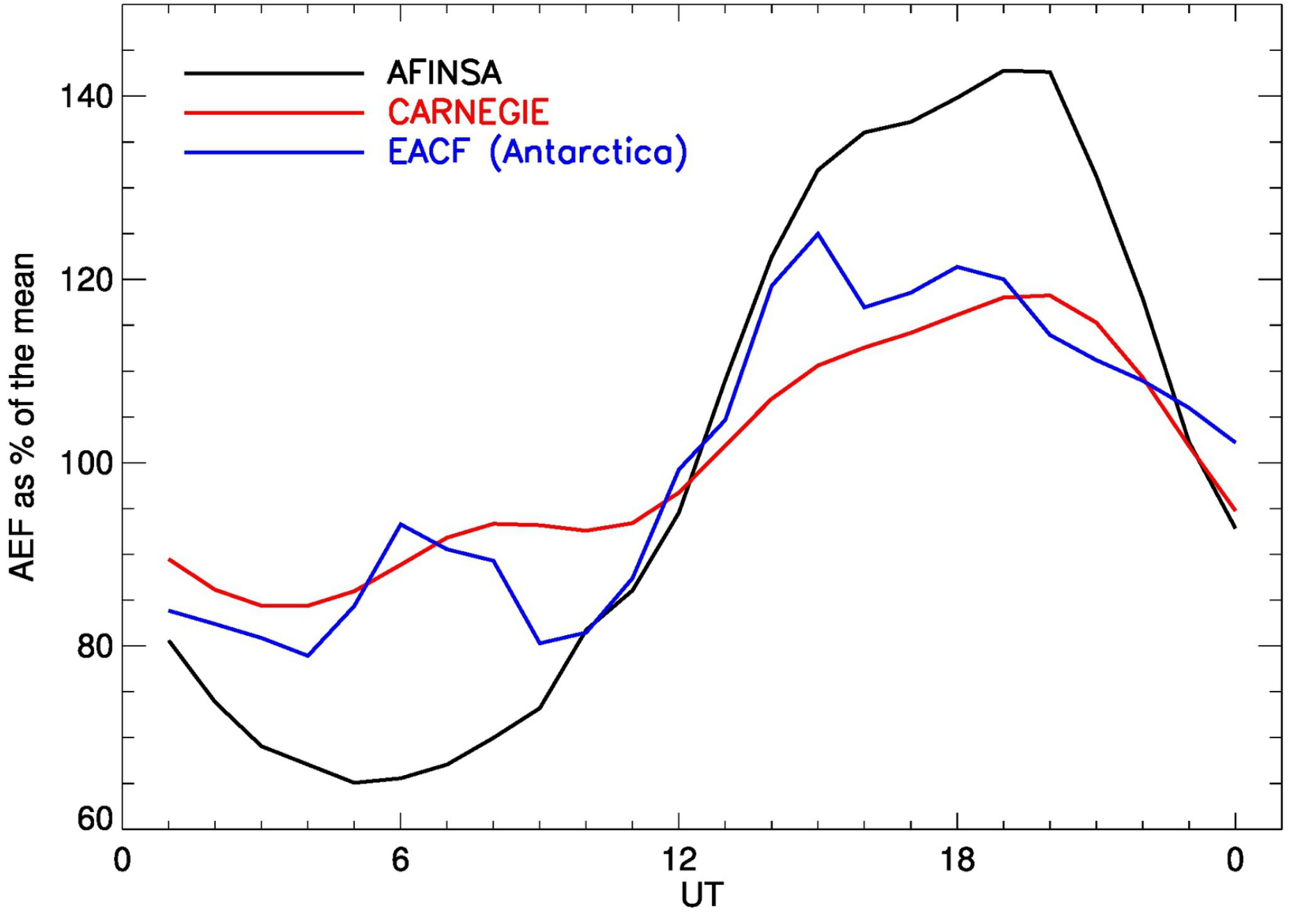
AFINSA
CARNEGIE
EACF (Antarctica)
AEF as % of the mean
140
120
100
80
60
0
6
12
18
0
UT

Figure 10